

Chapter 5

Fractal Basin Boundaries

Dissipative dynamical systems often possess multiple coexisting attractors. The set of initial conditions leading to trajectories landing on an attractor is the basin of attraction of this attractor. Each attractor thus has its own basin, which is invariant under the dynamics, since images of every point in the basin still belong to the same basin. The basins of attraction are separated by boundaries. We shall demonstrate that it is common for nonlinear systems to have *fractal basin boundaries*, the dynamical reason for which is nothing but transient chaos on the boundaries. In fact, fractal basin boundaries contain one or several nonattracting chaotic sets.

We will describe the basic dynamical properties of basin boundaries and introduce the main types of fractal basin boundaries. In general, a basin boundary can be characterized by its box-counting dimension and the predictability of the final state; the latter is quantified by the *uncertainty exponent*. The issue of how fractal basin boundaries can arise as a system parameter changes will be discussed. Topics such as Wada basin boundaries (common fractal basin boundaries among at least three basins of attraction) and sporadically fractal basin boundaries (boundaries consisting of smooth curves or surfaces and nondifferentiable components) will be addressed. Attention will also be paid to riddled basins in symmetrical dynamical systems, an extreme type of basin structure that practically defies predictability of the final state. The consequences of symmetry-breaking perturbations will be discussed.

A primary goal of science is to make predictions based on a set of physical laws. A question of natural concern, due to the inevitable error in the specification of the initial condition, is whether the final state of a trajectory can be predicted from an initial condition chosen in the vicinity of a basin boundary. The various situations to be discussed in this chapter illustrate that the prediction of the final state can be extremely difficult and sometimes practically impossible even for relatively simple deterministic systems.

5.1 Basin Boundaries: Basics

To gain intuition, we consider the following simple physical system in which a particle of unit mass moves under conservative force determined by a one-dimensional potential function $V(x)$. In the two-dimensional phase space $(x, v \equiv dx/dt)$, the equations of motion are

$$\frac{dx}{dt} = v, \quad \frac{dv}{dt} = -\gamma v - \frac{dV}{dx}, \quad (5.1)$$

where we assume that there is a frictional force proportional to the velocity of the particle and $\gamma > 0$ is a dissipation parameter. To create multiple coexisting attractors, consider the class of symmetric double-well potentials, as schematically illustrated in Fig. 5.1a. The two potential wells are located at $x_{\pm} = \pm a$, and there is a potential barrier at $x_b = 0$. For a particle in the vicinity of a well, if the initial velocity is small such that the initial energy of the particle is not large enough for it to overcome the potential barrier, it will approach asymptotically the bottom of the well, due to the friction. Each well is thus an attractor and there are two attractors in the phase space, located at $(x, v) = (\pm a, 0)$. To understand the structure of the basins of attraction and the basin boundary, we notice that if a still particle sits precisely on the top of the

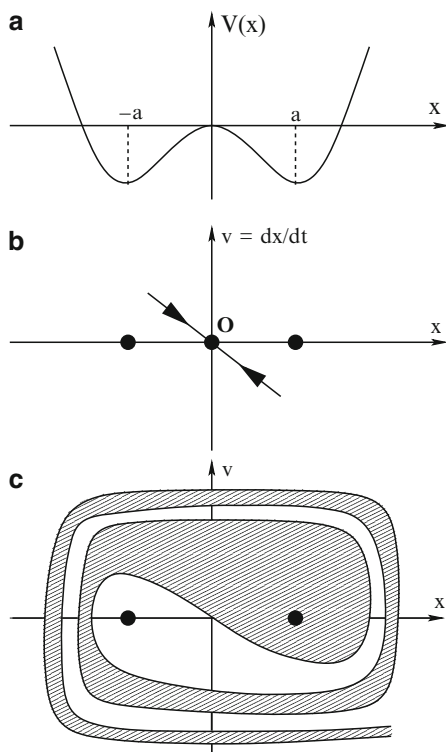


Fig. 5.1 (a) Double-well potential $V(x)$, (b) Hyperbolic point $O = (0, 0)$ and a linear segment of its stable manifold belonging to the boundary between the basins of attraction of the two attractors located at $(x, v) = (\pm a, 0)$. (c) Schematic illustration of the basin boundary and the two basins of attraction

barrier, it will remain there forever, although an arbitrarily small perturbation, either in its position or velocity, or a combination of the two, can move the particle to one of the wells. Thus the point $\mathbf{O} \equiv (0, 0)$ is an unstable fixed point on the basin boundary.

Now consider a particle initially located in the right well but near \mathbf{O} . If it is given a small initial velocity in the $-x$ direction, it may or may not overcome the potential barrier. There then exists a velocity for which the particle stops precisely at \mathbf{O} . Likewise, for a particle initially in the left well but near \mathbf{O} , there exists a small initial velocity in the $+x$ direction that lands the particle precisely at \mathbf{O} . In the two-dimensional phase space, there then exists a set of initial conditions lying on a one-dimensional curve that is approximately linear¹ near \mathbf{O} , which approaches \mathbf{O} asymptotically, as shown schematically in Fig. 5.1b. In the terms of dynamical systems, the one-dimensional curve is the stable manifold of the saddle point \mathbf{O} . Since points on the curve do not approach any of the two attractors, it is the basin boundary. The reasoning thus suggests that in situations in which multiple attractors coexist in invertible systems, the basin boundary is the stable manifold of some unstable invariant set on the boundary.

While the basin boundary is approximately linear near the unstable fixed point \mathbf{O} , it curves away from \mathbf{O} , due to nonlinearity. For the simple example in Fig. 5.1, the boundary crosses the x -axis an infinite number of times. This can be seen by noticing that away from an attractor, say from the one on the right well in the $+x$ direction, the force becomes attractive. There then exists a set of \bar{x} values, where $\bar{x} > a$, for which the amount of force is just right to place an initially still particle right at the top of the potential barrier. The points $(\bar{x}, 0)$ are thus on the basin boundary. This leads to basins consisting of strips near the x -axis for $|x|$ large, as shown schematically in Fig. 5.1c. A basin of attraction typically possesses an infinite phase-space volume.²

The simple mechanical example in Fig. 5.1 illustrates that when the invariant set on the basin boundary is simple, e.g., an unstable periodic orbit, the boundary is smooth. One can imagine the situation that there is a nonattracting chaotic set on the basin boundary. Since the stable manifold of the chaotic set is a fractal set, the boundary becomes fractal.

5.2 Types of Fractal Basin Boundaries

In typical dynamical systems, i.e., systems whose behaviors are not due to any special properties such as symmetry, there are at least three known types of fractal basin boundaries, [294] described in the subsequent subsections.

¹ Near \mathbf{O} , we have $V \approx -s^2x^2/2$. The solution to (5.1) is $x(t) = c_+e^{\lambda_+t} + c_-e^{\lambda_-t}$ with $\lambda_{\pm} = -\gamma/2 \pm (s^2 + \gamma^2/4)^{1/2}$. Thus, for $c_+ = 0$, we have $v(t) = \lambda_-x(t) \sim e^{\lambda_-t}$ and $x(t) \rightarrow 0, v(t) \rightarrow 0$ as $t \rightarrow \infty$, along the line $v = \lambda_-x$.

² Choose a phase-space region R of nonzero volume that encloses an attractor. That the system is dissipative means that the inverse dynamics is volume-expanding. Since R is completely in the basin of attraction, all its preimages are in the basin as well. In the limit $t \rightarrow -\infty$, the volume of the preimage becomes infinite.

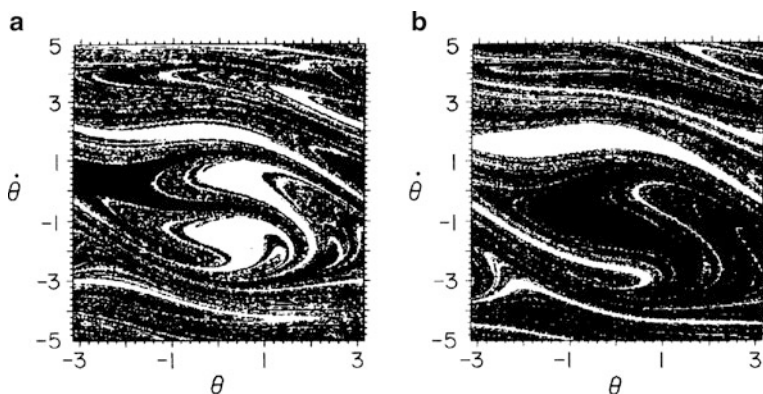


Fig. 5.2 Basins of attraction for the forced damped pendulum (5.2) on the stroboscopic surface of section $(\theta, \dot{\theta})$ defined by $t = 2n\pi$ ($n = 0, 1, \dots$). (a) For $\gamma = 0.1$, $f_0 = 1.2$, there is a fixed-point attractor at $\theta = -2.2055$ and $\dot{\theta} = 0.3729$. Black regions denote initial conditions that go to this attractor. There is another attractor in the blank region. (b) For $f_0 = 2.0$, the attractor in the black basin of attraction is located at $\theta = -0.8058$ and $\dot{\theta} = 0.9375$ [296] (with kind permission from Elsevier Science)

5.2.1 Filamentary Fractal Boundaries

Filamentary fractal boundaries are boundaries locally consisting of a Cantor set of smooth curves or surfaces. This situation typically occurs in invertible dynamical systems, where the asymptotic invariant sets on the boundary contain a chaotic saddle [491, 794]. Examples are shown in Fig. 5.2a, b for the following periodically forced damped pendulum [296]:

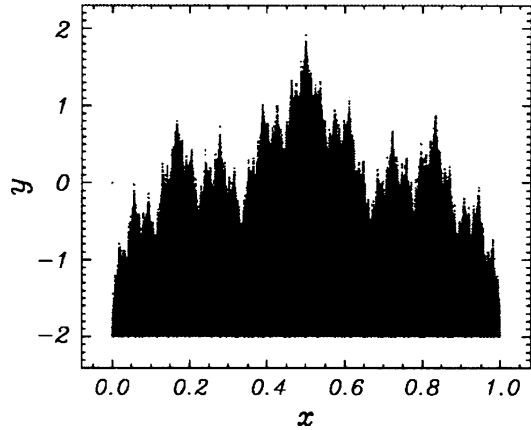
$$\frac{d^2\theta}{dt^2} + \gamma \frac{d\theta}{dt} + \sin\theta = f_0 \cos t, \quad (5.2)$$

where γ is a frictional coefficient and f_0 is the forcing amplitude. Such boundaries may also contain nonfractal parts, e.g., in regions about the attractors. In certain systems, these two types of boundary behaviors are intertwined on arbitrarily fine scales. For any area that contains a fractal part of the boundary, there is a subarea that contains only smooth parts of the boundary. Such fractal boundaries are called *intertwined boundaries*.

5.2.2 Continuous Fractal Boundaries

Continuous fractal boundaries are boundaries that are a continuous but nowhere differentiable curve or surface. An illustrative example is the following class of noninvertible two-dimensional maps: [511, 564]:

Fig. 5.3 For the two-dimensional map (5.3), the basin boundary between the $y = \pm\infty$ attractors. The parameters are $a = 3$ and $\lambda = 1.5$. The boundary is continuous but nowhere differentiable, as represented by a Weierstrass curve [511] (with kind permission from Elsevier Science)



$$\begin{aligned} x_{n+1} &= ax_n \text{ mod } (1), \\ y_{n+1} &= \lambda y_n + \cos(2\pi x_n), \end{aligned} \tag{5.3}$$

where $a > \lambda > 1$ and a is an integer. Since $\lambda > 1$, almost all initial conditions lead to trajectories that go to $y = \pm\infty$, which can be regarded as two attractors. The term $\cos(2\pi x_n)$ in the y -equation entails that the basin boundary near $y = 0$ can be complicated. Indeed, an explicit expression for the boundary curve can be obtained [511, 564]:

$$y = g(x) = - \sum_{j=1}^{\infty} \lambda^{-j} \cos(2\pi a^{j-1} x). \tag{5.4}$$

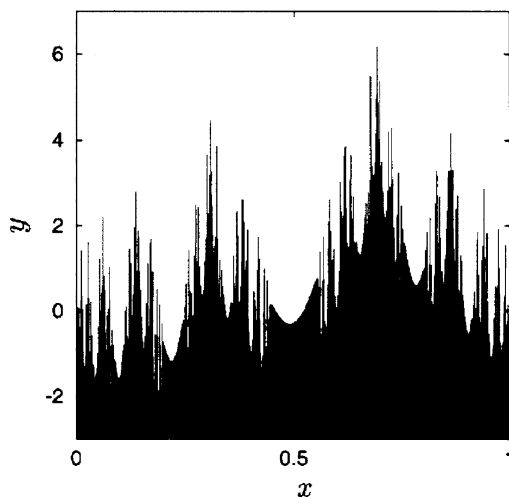
A direct substitution into (5.3) shows that $y = g(x)$ is an invariant curve, i.e., $y_n = g(x_n)$ and $y_{n+1} = g(x_{n+1})$. The curve thus contains an invariant set, a chaotic repeller. The curve $y = g(x)$ is continuous but nowhere differentiable because dy/dx diverges for every value of x . The curve in (5.4) in fact has the box-counting dimension $D_0 = 2 - (\ln \lambda)/(\ln a)$, and is called a *Weierstrass curve*. An example is shown in Fig. 5.3.

5.2.3 Sporadically Fractal Boundaries

In a two-dimensional map, basin boundaries of the sporadically fractal type can be described by a function $g(x)$ that is smooth except for a set of x values of zero measure (i.e., zero length), but nevertheless has a box-counting dimension larger than 1. An illustrative example is [346, 651]

$$\begin{aligned} x_{n+1} &= f(x_n), \\ y_{n+1} &= \lambda y_n + \sin(2\pi x_n), \end{aligned} \tag{5.5}$$

Fig. 5.4 Example of a sporadically fractal basin boundary from the two-dimensional map (5.5) [346] (Copyright 1999, the American Physical Society)



where $\lambda > 1$ and $f(x)$ is a noninvertible one-dimensional map. Part of the basin boundary is shown in Fig. 5.4. It can be seen that the boundary consists mostly of smooth parts but with sporadic “spikes” along the curve. Sporadically fractal basin boundaries can arise in the context of chaotic phase synchronization in continuous-time dynamical systems.

If a dynamical system possesses a special property such as simple symmetry, the topology of the basins of attraction can be quite different from those seen in typical systems.

5.2.4 Riddled Basins

If the symmetry leads to an invariant subspace in the phase space, where there is a chaotic attractor, the basin of attraction of this chaotic attractor can be riddled with holes that belong to the basin of another attractor, provided that such an attractor exists outside the invariant subspace [11]. A riddled basin thus contains no open sets (e.g., areas in two dimensions or volumes in three dimensions), in contrast to fractal basins. Physically, the presence of a riddled basin means that for every initial condition that goes to the chaotic attractor in the invariant subspace, there are initial conditions *arbitrarily nearby* that lead to trajectories to the other coexisting attractor. Prediction of the asymptotic attractor for a given initial condition thus becomes practically impossible. An example of a riddled basin has been found experimentally, as shown in Fig. 1.18. A numerically obtained riddled basin can be seen in Fig. 5.5, in which a particle of unit mass moves in a planar potential given by

$$V(\mathbf{x}) = (1 - x^2)^2 + (y^2 - a^2)^2(x - d) + b(y^2 - a^2)^4,$$

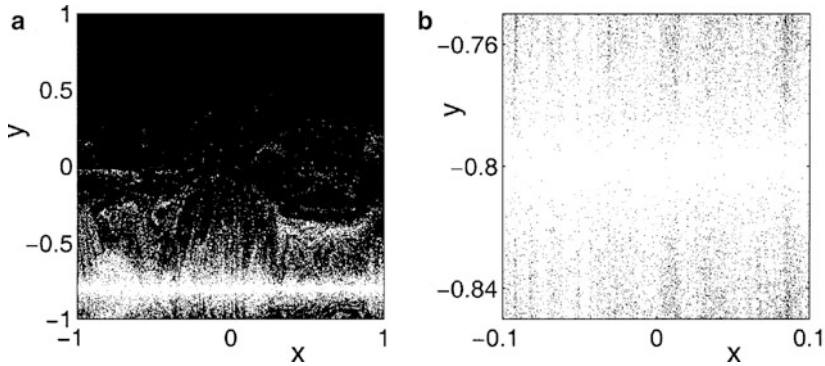


Fig. 5.5 Riddled basins. (a) Solution of (5.6) with parameters $f_0 = 2.3$, $\gamma = 0.05$, $\omega = 3.5$, $a = 0.8$, $b = 0.008$, and $d = -0.19$. Black dots represent points in the basin of the attractor at $y = a$, $v_y = 0$. (b) A magnification of part of (a) near the invariant subspace at $y = -a$ and $v_y = 0$. One can see that arbitrarily close to the attractor at $y = -a$ there are points belonging to the attractor at $y = a$ [448] (Copyright 1995, the American Physical Society)

where a , b , and d are parameters. The particle is also subject to friction and periodic forcing. The equation of motion is

$$\frac{d^2 \mathbf{x}}{dt^2} = -\gamma \frac{d\mathbf{x}}{dt} - \nabla V(\mathbf{x}) + f_0 \sin(\omega t) \mathbf{e}_x, \quad (5.6)$$

where $\mathbf{x} \equiv (x, y)$, γ is the frictional coefficient, and \mathbf{e}_x is the unit vector in x . There are two invariant subspaces determined by $y = \pm a$ and $v_y = 0$ in which the dynamics are governed by the forced double-well problem (Duffing's equation). For proper choices of the parameters a , b , and d , the basins of the chaotic attractors in the symmetric invariant subspaces are both riddled, as shown in Fig. 5.5. When all basins are riddled by the rest, as is the case here, the basins are said to be *intermingled* [448]. Note, however, that riddled basins rely on the symmetry of the system. A small amount of symmetry-breaking leads to a catastrophic bifurcation whereby a riddled basin immediately becomes fractal with open areas.

A recent review by Aguirre et al. [7] on fractal basin boundaries gives a comprehensive treatment of the topic and presents a large number of applications. Our focus here will be on the interplay between fractal basin boundaries and transient chaos.

5.3 Fractal Basin Boundaries and Predictability

The box-counting dimension D_{b0} can be used to characterize the boundary. Let D be the dimension of the phase space. Since the boundary divides the phase space, we have $D - 1 \leq D_{b0} \leq D$. A question of interest in a practical situation is, what are the

physical meaning and consequences of having fractal basin boundaries of dimension D_{b_0} ? In particular, suppose we have two D -dimensional dynamical systems with basin boundaries of dimensions $D_{b_0}^{(1)}$ and $D_{b_0}^{(2)}$, where $D - 1 < D_{b_0}^{(1)} < D_{b_0}^{(2)} < D$. What are the physical manifestations of the difference in the dimensions?

The answer to the question concerns the predictability of the asymptotic attractor, or the final state, given an initial condition and a set of parameters, specifications of which inevitably contain uncertainties. One is thus interested in how the predictability can possibly be improved when the uncertainties are reduced. For concreteness, consider the situation in which parameters of the system are fixed and the major uncertainty in specifying the system state occurs in the initial condition. Let ε be this uncertainty and let $f(\varepsilon)$ be the probability of making an error in the prediction of the final state, which depends on ε . As ε is reduced, one expects to be able to predict the final state more accurately, so $f(\varepsilon)$ will decrease. Of interest is thus the scaling relation between $f(\varepsilon)$ and ε . In general, we have [289, 511, 528]

$$f(\varepsilon) \sim \varepsilon^\alpha, \quad (5.7)$$

where the scaling exponent $\alpha > 0$ is called the *uncertainty exponent* [289, 511]. For fractal boundaries, α satisfies the inequality

$$\alpha < 1, \quad (5.8)$$

and $\alpha = D - D_{b_0}$.

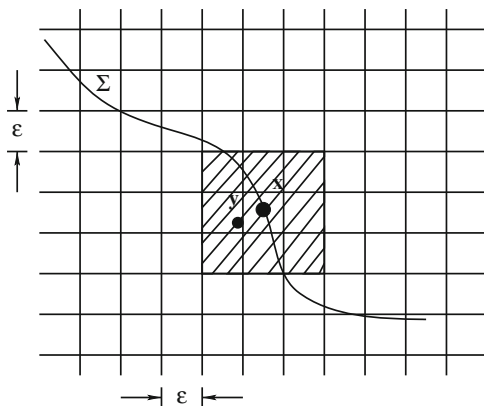
For a smooth basin boundary of dimension $D_{b_0} = D - 1$ in the D -dimensional phase space, the scaling law (5.7) can be observed straightforwardly, as follows. Since an initial condition is specified with precision ε , we can associate each initial condition with a D -dimensional ball of radius ε , centered at the initial condition. If a ball is located completely in the basin of attraction of an attractor, the fates of all initial conditions in the ball are certain: they all go to this attractor. Only when the ball crosses a boundary is a wrong prediction of the final state possible, because initial conditions contained in the ball can now go to different attractors. The probability of making an error in prediction is thus proportional to the phase-space volume contained within ε of the boundary, which is $S_0\varepsilon \sim \varepsilon$, where S_0 is the $(D - 1)$ -dimensional volume of the basin boundary. We thus have

$$f(\varepsilon) \sim \varepsilon,$$

which gives $\alpha = 1 = D - D_{b_0}$.

For a fractal basin boundary Σ of dimension $D - 1 \leq D_{b_0} \leq D$, let $V(\varepsilon)$ be the volume of all points within distance ε of Σ . To derive a relation between the uncertainty exponent and the dimension D_{b_0} , one can estimate the upper and lower bounds of $V(\varepsilon)$ using different covering schemes [511]. Specifically, imagine that we cover the phase space with a grid of boxes of edge length ε . Each boundary point \mathbf{x} of Σ is in a box that typically has $3^D - 1$ neighboring boxes, points in which can be within ε of \mathbf{x} . That is, a point \mathbf{y} within ε of \mathbf{x} can be in one of the 3^D boxes (including the box that contains \mathbf{x} itself), as shown schematically in Fig. 5.6. An upper bound

Fig. 5.6 A grid of boxes of size ϵ covering basin boundary Σ . In two dimensions, each box containing a boundary point \mathbf{x} has $3^2 - 1 = 8$ neighboring boxes, which contains points that can be within ϵ of \mathbf{x} . Any point \mathbf{y} within \mathbf{x} can be in one of the 3^2 boxes. In a D -dimensional phase space, the number of boxes satisfying this requirement is 3^D



to $V(\epsilon)$ is a coverage using $3^D N(\epsilon)$ boxes, where $N(\epsilon)$ is the number of ϵ -boxes needed to cover the boundary:

$$V(\epsilon) \leq 3^D N(\epsilon) \epsilon^D. \tag{5.9}$$

Now let us choose a smaller grid covering Σ such that any two points in a box are separated by a distance at most ϵ , which can be achieved using boxes of edge length ϵ/\sqrt{D} . The number of such boxes required to cover the entire boundary is $N(\epsilon/\sqrt{D})$. In this case, every box in the coverage is within distance ϵ to the boundary Σ . Therefore, we have

$$V(\epsilon) \geq (\epsilon/\sqrt{D})^D N(\epsilon/\sqrt{D}). \tag{5.10}$$

The number $N(\epsilon)$ of boxes needed to cover Σ scales (see (1.19)) with ϵ as $N(\epsilon) \sim \epsilon^{-D_{b0}}$. We thus have, from (5.9) and (5.10),

$$V(\epsilon) \sim \epsilon^{D-D_{b0}}. \tag{5.11}$$

Since $f(\epsilon) \sim V(\epsilon)$, we have $f(\epsilon) \sim \epsilon^\alpha$ with

$$\alpha = D - D_{b0}. \tag{5.12}$$

The uncertainty exponent is the difference between the dimension of the phase space and that of the boundary.

The physical interpretation of the scaling relation (5.7) is as follows. Suppose one wishes to reduce the probability of error in the prediction of the final state by improving the precision in the specification of the initial conditions. If the basin boundary is smooth so that $\alpha = 1$, a reduction in ϵ results in an equal amount of reduction in $f(\epsilon)$. For fractal basin boundaries, where $\alpha < 1$, a more precise specification of the initial conditions results in a much smaller improvement in the probability of predicting the final attractor correctly. In the extreme case in which $\alpha \approx 0$, a vast reduction in the uncertainty of specifying the initial conditions will

result in almost no improvement in one's ability to determine the final state, which can occur, for example, with riddled basins. In this sense, prediction is more difficult for basin boundaries whose dimension values D_{b0} are larger [830].

The uncertainty exponent can be expressed in terms of the properties of the nonattracting chaotic set embedded in the boundary. In invertible systems, fractal basin boundaries typically contain both smooth parts and the stable manifold of a chaotic saddle. Since the dimension of the union of two sets is that of the set with higher dimension, we have $D_{b0} = D_{s0}$, where D_{s0} denotes the box-counting dimension of the stable manifold. For two-dimensional maps ($D = 2$), we have $D_{s0} = 1 + D_0^{(1)}$, where $D_0^{(1)}$ is the partial box-counting dimension along the unstable direction. These considerations lead to

$$\alpha = 1 - D_0^{(1)} \approx \frac{\kappa}{\lambda_1}. \quad (5.13)$$

The approximate equality follows from (2.76) and the estimate $D_0^{(1)} \approx D_1^{(1)}$, and states that the uncertainty exponent can be approximated by the ratio of the escape rate and the largest Lyapunov exponent of the chaotic saddle embedded in the boundary. For the case of sporadic and riddled basins, see (5.22) and (5.29).

Numerically, the uncertainty exponent α can be calculated as follows. Given a phase-space region containing some basin boundaries, we randomly choose a pair of initial conditions \mathbf{x}_0 and $\mathbf{x}_0 + \boldsymbol{\varepsilon}$, where $\boldsymbol{\varepsilon}$ is a small perturbation. We then determine whether these two initial conditions go to the same attractor. If yes, \mathbf{x}_0 is called *certain* with respect to the perturbation $\boldsymbol{\varepsilon}$. Otherwise, \mathbf{x}_0 is *uncertain*. The probability $f(\boldsymbol{\varepsilon})$ of making an error in the prediction of the final attractor can be estimated by choosing a large number N_0 of initial conditions in the phase-space region according to some smooth probability distribution. For example, if N_u is the number of uncertain initial conditions with respect to $\boldsymbol{\varepsilon}$, we have $f(\boldsymbol{\varepsilon}) \approx N_u/N_0$. The uncertainty exponent is approximated by the slope of a linear fit in the plot of $f(\boldsymbol{\varepsilon})$ versus $\boldsymbol{\varepsilon}$ on a logarithmic scale.

To illustrate the computation of the uncertainty exponent, we take the two-dimensional map [511]:

$$\begin{aligned} \theta_{n+1} &= \theta_n + 1.32 \sin(2\theta_n) - 0.9 \sin(4\theta_n) - x_n \sin(\theta_n), \\ x_{n+1} &= -J_0 \cos(\theta_n), \end{aligned} \quad (5.14)$$

where x can be regarded as the radial distance from the center of an annulus, θ is an angle variable such that θ and $\theta + 2\pi$ are equivalent, and J_0 is a parameter. (It is this model whose quasipotential is shown in Fig. 4.6 and which has been used for the illustration of noise-induced chaos in Fig. 4.10.) The system is invariant under the symmetry $\theta \rightarrow 2\pi - \theta$. The determinant of the Jacobian matrix is $J_0 \sin^2(\theta) < 1$ (for $J_0 < 1$). There are two attractors, located at $x = -J_0$, $\theta = 0$ (denoted by A_-) and $x = J_0$, $\theta = \pi$ (denoted by A_+), respectively. The boundaries separating the basins of attraction of the two attractors are fractal, as shown in Fig. 5.7a for $J_0 = 0.3$, where black dots represent the basin of attraction of A_+ . To compute the fraction $f(\boldsymbol{\varepsilon})$ of

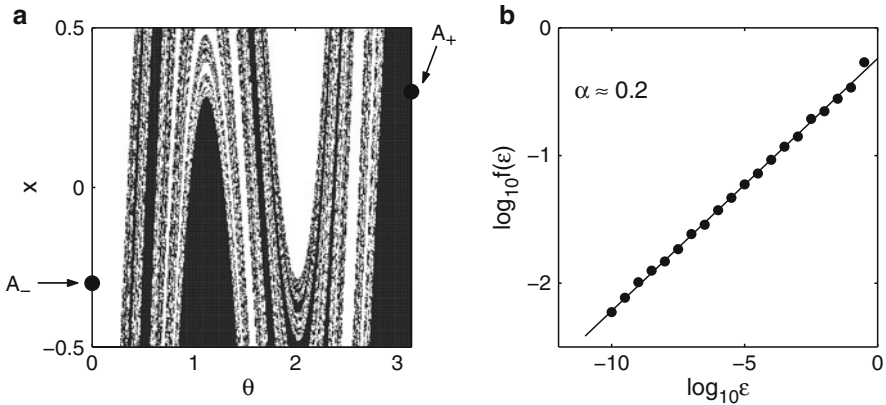


Fig. 5.7 (a) Fractal basin boundaries for the map (5.14) with $J_0 = 0.3$. The two point attractors are denoted by A_- and A_+ , respectively. (b) Plot of $f(\epsilon)$ versus ϵ on a logarithmic scale. The uncertainty exponent is estimated to be $\alpha \approx 0.2$ [511] (with kind permission from Elsevier Science)

uncertain initial conditions, we fix a line segment $\theta \in [0, \pi]$ at $x = 0$, choose a pair of initial conditions at ϵ -distance apart randomly from this line, and numerically determine whether the two initial conditions approach different attractors. For every ϵ -value the number N_0 of the initial-condition pairs is increased until the number of uncertain initial conditions reaches 1,000, so that $f(\epsilon) \approx 1,000/N_0$. Figure 5.7b shows the algebraic scaling between $f(\epsilon)$ and ϵ . A least-squares fit gives a slope of about 0.2, which is the uncertainty exponent α . The dimension of the basin boundary is thus $D_{b0} = 2 - \alpha \approx 1.8$.

To appreciate the value of the uncertainty exponent, say we make efforts to reduce the uncertainty in the specification of the initial condition by five orders of magnitude. Then $\alpha \approx 0.2$ means that the probability of making an error in predicting the final attractor is reduced only by a factor of $(10^{-5})^{0.2} = 0.1$. Thus the presence of the fractal basin boundaries makes predicting the final state difficult.

In experimental situations or in high-dimensional systems it is often difficult to determine the initial conditions. One can then attempt to evaluate the uncertainty exponent using random variations in the parameter space. A question is whether the value of the uncertainty exponent so obtained is the same as that obtained using random perturbations in initial conditions. The answer is affirmative because a parameter variation can be regarded as being equivalent to a perturbation in the initial conditions. Specifically, consider a D -dimensional map $\mathbf{x}_{n+1} = \mathbf{f}(\mathbf{x}_n, \mathbf{p})$, where \mathbf{p} denotes a set of parameters. Assume that the system under the initial condition \mathbf{x}_0 and parameter value \mathbf{p}_0 goes to one attractor. The standard approach is to take a slightly different initial condition $\mathbf{x}'_0 = \mathbf{x}_0 + \Delta\mathbf{x}$ at fixed parameter \mathbf{p}_0 . The image point is then $\mathbf{f}(\mathbf{x}'_0, \mathbf{p}_0)$. Alternatively, one can take a slightly different set of parameter values $\mathbf{p}'_0 = \mathbf{p}_0 + \Delta\mathbf{p}$, at the same initial condition, which leads to $\mathbf{f}(\mathbf{x}_0, \mathbf{p}'_0)$. The image points are identical if $\partial\mathbf{f}/\partial\mathbf{p}|_{\mathbf{x}_0, \mathbf{p}_0} \cdot \Delta\mathbf{p} = \partial\mathbf{f}/\partial\mathbf{x}|_{\mathbf{x}_0, \mathbf{p}_0} \cdot \Delta\mathbf{x}$. We expect then the uncertainty exponents computed with respect to perturbations in the parameter and

in the phase space to be identical. In fact, one of the first determinations of fractal basin boundaries [528] was done using parameter perturbations. This parameter and phase-space equivalence was also used to study basin structures in coupled-map lattice systems [462–464].

5.4 Emergence of Fractal Basin Boundaries

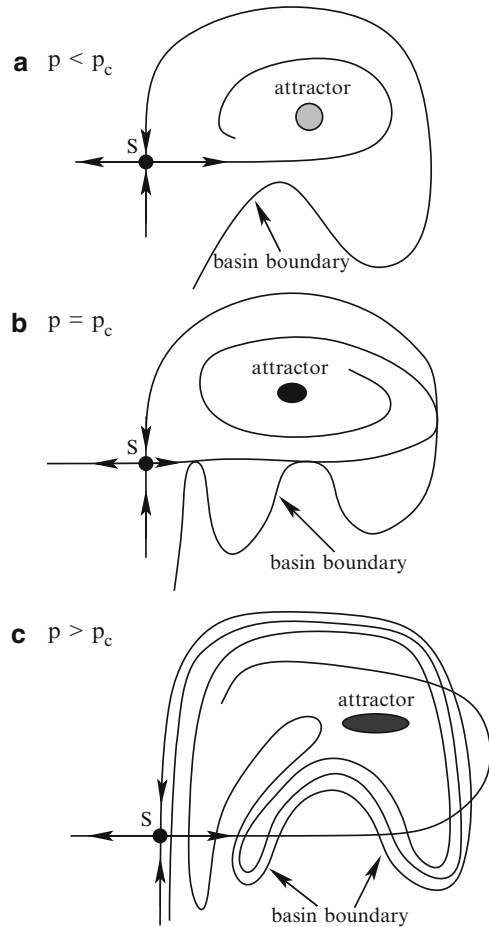
5.4.1 Basin Boundary Metamorphoses and Accessible Orbits

The typical dynamical mechanism that creates fractal basin boundaries from a smooth boundary is homoclinic or heteroclinic tangencies, as schematically illustrated in Fig. 5.8, where p is a bifurcation parameter. Throughout the bifurcation there is an unstable periodic orbit (e.g., a saddle fixed point), denoted by S . The stable manifold of S is the basin boundary between an attractor to its right (shown) and another attractor (not shown). As p is changed through the bifurcation point p_c , both the basin boundary and the attractor evolve. For $p < p_c$, the basin boundary is smooth (Fig. 5.8a). Homoclinic tangencies between the stable and the unstable manifolds of S occur at p_c , as shown in Fig. 5.8b. For $p > p_c$, the homoclinic crossings between the stable and the unstable manifolds of S imply a Smale horseshoe-type dynamics (Sect. 1.2.2.1) in the vicinity of S . As a result, a chaotic saddle is created that contains the set of intersecting points between the stable and the unstable manifolds. The stable foliation, and equivalently the basin boundary, becomes fractal. The bifurcation from smooth to fractal basin boundaries is called a *smooth-to-fractal basin boundary metamorphosis* [296].

A basin boundary metamorphosis is typically accompanied by a change in the unstable periodic orbits on the basin boundary that is *accessible* to the attractor [296]. A boundary point \mathbf{P} is accessible from a region if there is a curve of *finite length* that connects \mathbf{P} to a point in the interior of the region such that no point on the curve belongs to the boundary except point \mathbf{P} . From Fig. 5.8, we see that the saddle fixed point S is accessible to the attractor for $p < p_c$. However, for $p > p_c$, the fractal foliations of the stable manifold entail that it is not possible to connect S to a point on the attractor through a curve of finite length. The fixed point S is thus inaccessible to the attractor for $p > p_c$. Instead, a new unstable periodic orbit, one of the infinite number of those embedded in the chaotic saddle, becomes accessible to the attractor.

The change in the accessible unstable periodic orbits can be demonstrated [296] using the Hénon map with a positive Jacobian J . The map has one attractor at infinity. For fixed J , as the bifurcation parameter a is increased through the value $a_1 = -(J+1)^2/4$, a saddle-node bifurcation occurs, creating an attracting fixed point and a saddle point, which separate from each other for $a > a_1$. For a slightly above a_1 , the map has two attractors: one at the attracting point and another at infinity. The basin boundary is the stable manifold of the saddle, as shown in Fig. 5.9a for $a = 1.150$. The saddle point is accessible to the period-1 attractor. As a is increased

Fig. 5.8 Dynamical mechanism that creates fractal basin boundaries. (a) Smooth basin boundary for $p < p_c$, (b) homoclinic tangencies for $p = p_c$, and (c) homoclinic crossings for $p > p_c$. The stable foliations and, equivalently, the basin boundaries, become fractal for $p > p_c$



further, a metamorphosis occurs, which converts the smooth boundary into a fractal. An example of the fractal basin boundary is shown in Fig. 5.9b for $a = 1.395$. We see that, because of the fractal foliation of the basin boundary, the original saddle fixed point is no longer accessible to the attractor, which for this parameter value has already evolved into a period-2 attractor through a period-doubling bifurcation. The accessible orbit on the boundary becomes a hyperbolic periodic orbit of period 4.

We can imagine that as the parameter is varied further, this new accessible unstable periodic orbit can also have homoclinic tangencies, after which it becomes inaccessible. The subsequent homoclinic intersections mean that the basin boundary must necessarily undergo another metamorphic change to a fractal one that is distinct from the original boundary. This is a *fractal-to-fractal basin boundary metamorphosis*, after which a different unstable periodic orbit on the boundary becomes accessible, as illustrated in Fig. 5.9c for $a = 1.405$. We see that the fractal boundary appears to be quite distinct from that in Fig. 5.9b, and the originally accessible period-4 orbit in Fig. 5.9b is replaced by a period-3 orbit in Fig. 5.9c.

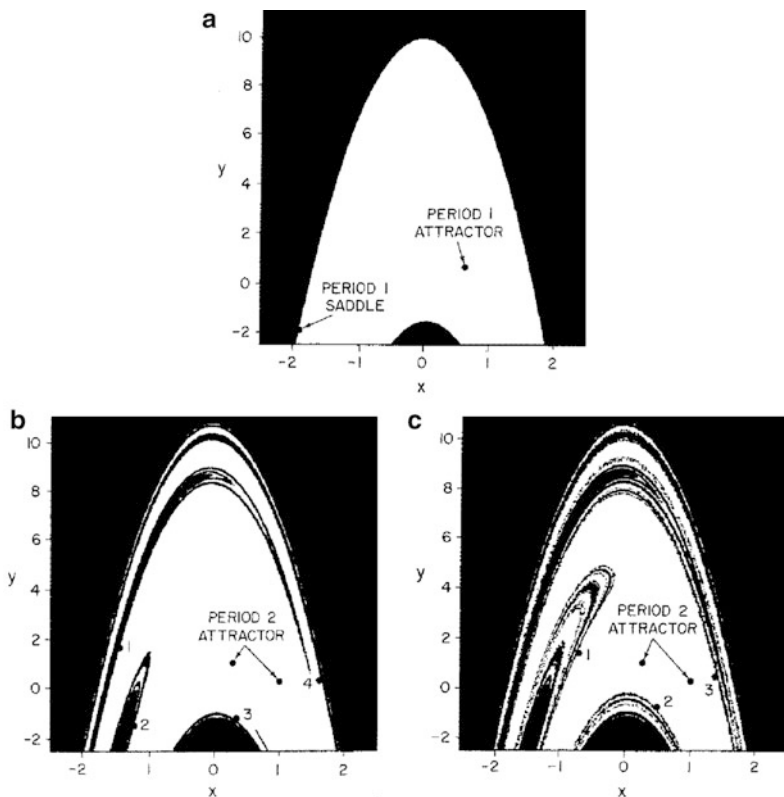


Fig. 5.9 Basin boundary metamorphosis. For the Hénon map $(x_{n+1}, y_{n+1}) = (a - x_n^2 - Jy_n, x_n)$ for $J = 0.3$, (a) smooth basin boundary for $a = 1.150$, where the accessible orbit on the boundary is the saddle fixed point created at a saddle-node bifurcation. (b) Fractal basin boundaries for $a = 1.395$ after a smooth-to-fractal basin boundary metamorphosis. The accessible orbit on the boundary is now a period-4 orbit. (c) Qualitatively different fractal basin boundaries after a fractal-to-fractal boundary metamorphosis with a new period-3 accessible orbit for $a = 1.405$. The numerals in (b) and (c) denote the accessible periodic orbits in the sequences of iterations [296] (with kind permission from Elsevier Science)

5.4.2 Dimension Changes at Basin Boundary Metamorphoses

As the basin boundary changes characteristically, e.g., from smooth to fractal or from fractal to fractal, we expect the dimension of the boundary to change *abruptly*. This can be seen qualitatively from Fig. 5.9a–c. Let a_{sf} and a_{ff} denote the parameter values for the smooth-to-fractal and the fractal-to-fractal boundary metamorphoses that create the fractal basin boundaries in Fig. 5.9b and c, respectively. For $a < a_{sf}$ (Fig. 5.9a), the boundary is a smooth curve in the two-dimensional phase space, so its box-counting dimension is $D_{b0} = 1$. For $a_{sf} < a < a_{ff}$ (Fig. 5.9b), the boundary is locally a Cantor set of smooth curves, so D_{b0} is between one and two. For $a > a_{ff}$ (Fig. 5.9c), the dimension is also a fractional (but distinct) value between one and two.

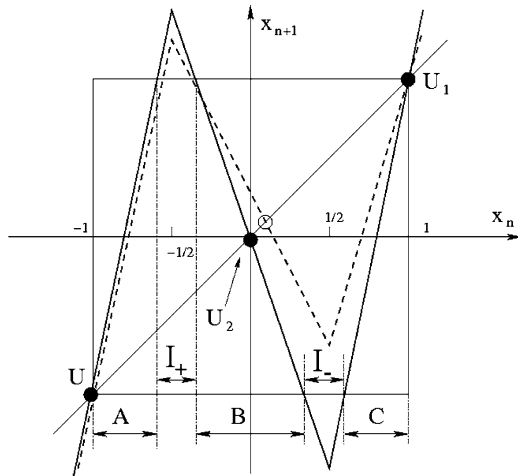


Fig. 5.10 One-dimensional map $x_{n+1} = f(x_n)$ with a positive peak at $x = -1/2$, which is always above 1 ($f(-1/2) > 1$), and a negative peak at $x = 1/2$. As the bifurcation parameter p changes from p_1 to p_2 , the negative peak moves from $f(1/2) > -1$ at $p = p_1$ (dashed lines) to $f(1/2) < -1$ at $p = p_2$ (solid lines). A smooth-to-fractal basin boundary metamorphosis occurs at $p = p_{sf}$ when $f(1/2) = -1$

To understand the abrupt dimension change associated with a basin boundary metamorphosis, an analyzable, piecewise linear, one-dimensional map $f(x)$ was introduced [578], as shown schematically in Fig. 5.10. The map has a positive peak at $x = -1/2$, which remains above one, $f(-1/2) > 1$, and a negative peak at $x = 1/2$ whose height varies as a bifurcation parameter p changes. In particular, say for $p = p_1$ the negative peak is above -1 (dashed line). As p is increased from p_1 to p_2 , the negative peak moves to below -1 (solid line). The map has three unstable fixed points: U at $x = -1$, U_1 at $x = 1$, and U_2 in the vicinity of $x = 0$. As p varies in the interval $[p_1, p_2]$, U and U_1 are fixed, but the location of U_2 can shift about $x = 0$. In this parameter interval of interest, the map has two attractors: one at $-\infty$ and another at $x = +\infty$. Since all points in $x < -1$ map to the attractor at $-\infty$ and all points in $x > +1$ go to the attractor at $+\infty$, the basin boundary must lie in the interval $[-1, 1]$.

Let p_{sf} denote the parameter value for which $f(1/2) = -1$, where $p_1 < p_{sf} < p_2$. For $p < p_{sf}$, since the negative peak at $x = 1/2$ stays within the square in Fig. 5.10, the basin of the attractor at $-\infty$ is $x < -1$. The basin of the attractor at $+\infty$ consists of the interval $x > 1$ and almost all points in $(-1, 1)$ except a Cantor set of measure zero. Let I_+ be the primary escape interval in $(-1, 1)$ such that $f(x) > 1$, which maps to $+\infty$. All preimages $\{f^{-n}(I_+)\}$ ($n = 1, \dots$) also map to $+\infty$. What is left in $(-1, 1)$ is a chaotic repeller. Despite the presence of the repeller, for $p < p_{sf}$ the basin boundary between the basins of the $\pm\infty$ attractors is a single point: $x = -1$.

As p increases through p_{sf} , the negative peak of $f(x)$ pokes through $f = -1$. Let I_- be the primary escape interval in $x \in (-1, 1)$ such that $f(x) < -1$, which maps to the attractor at $-\infty$. In addition, all preimages of I_- also map to $-\infty$. The basin of

attraction of the $-\infty$ attractor now consists of $x < -1$ and all preimages of I_- . The preimages of I_+ and I_- intertwine in a complicated way, and the chaotic repeller in $(-1, 1)$ that maps neither to $-\infty$ nor to $+\infty$ becomes the new basin boundary, which is a fractal. We see that there is a smooth-to-fractal basin boundary metamorphosis at $p = p_{sf}$, after which the basin boundary, which was originally the point $x = -1$, jumps far into the interior of the $+\infty$ basin. For p slightly larger than p_{sf} , there are subintervals of the $-\infty$ basin in $(-1, 1)$, which for $p < p_{sf}$ were entirely in the $+\infty$ basin. At the metamorphosis, the dimension of the basin boundary changes abruptly from zero to a fractional value. In particular, as p approaches p_{sf} from above, the box-counting dimension of the basin boundary is the dimension D_{b0}^{sf} of the invariant Cantor set in the limit of p 's approaching p_{sf} from below. As p increases further, the dimension decreases as the Cantor set becomes "thinner" in the interval $[-1, 1]$. The behavior of the dimension of the basin boundary through the metamorphosis is schematically illustrated in Fig. 5.11.

The dimension D_{b0} of the fractal basin boundary for $p \geq p_{sf}$ can be calculated as follows. Let $N(\epsilon)$ be the number of intervals of size ϵ needed to cover the boundary. As specified in Fig. 5.10, let A , B , and C denote the subintervals $[-1, -1/2 - \epsilon_2/2]$, $[-1/2 + \epsilon_2/2, 1/2 - \epsilon_1/2]$, and $[1/2 + \epsilon_1/2, 1]$, and let $N_A(\epsilon)$, $N_B(\epsilon)$, and $N_C(\epsilon)$ be the number of boxes of size ϵ needed to cover the subsets of boundary points in these subintervals, respectively. We have

$$N(\epsilon) = N_A(\epsilon) + N_B(\epsilon) + N_C(\epsilon). \tag{5.15}$$

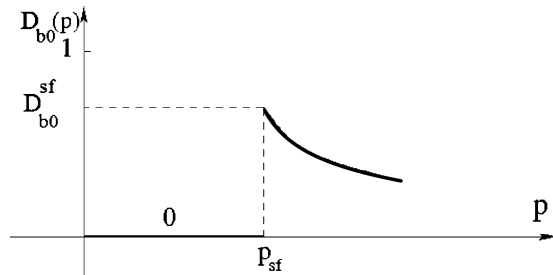
Self-similarities stipulate

$$N_A(\epsilon) = N \left[\frac{\epsilon}{1/4 - \epsilon_2/4} \right], \tag{5.16}$$

$$N_C(\epsilon) = N \left[\frac{\epsilon}{1/4 - \epsilon_1/4} \right],$$

$$N_B(\epsilon) = N \left[\frac{\epsilon}{(1/4 - \epsilon_2/4) + (1/4 - \epsilon_1/4)} \right].$$

Fig. 5.11 Schematic dependence of the box-counting dimension D_{b0} of the basin boundary through a smooth-to-fractal boundary metamorphosis



Substituting these into (5.15) and making use of the scaling $N(\varepsilon) \sim \varepsilon^{-D_{b0}}$, we obtain

$$\left(\frac{1}{4} - \frac{\varepsilon_1}{4}\right)^{D_{b0}} + \left(\frac{1}{2} - \frac{\varepsilon_1 + \varepsilon_2}{4}\right)^{D_{b0}} + \left(\frac{1}{4} - \frac{\varepsilon_2}{4}\right)^{D_{b0}} = 1. \quad (5.17)$$

As $p \rightarrow p_{sf}$ from above, $\varepsilon_1 \rightarrow 0$, and hence the value of the box-counting dimension $D_{b0}^{sf}(\varepsilon_2)$ for $p = p_{sf} + 0$ follows from (5.17) with $\varepsilon_1 = 0$. For p slightly above p_{sf} , so that $\varepsilon_1 > 0$ is small, we can write $D_{b0} = D_{b0}^{sf} - \eta$, where η is small. Substituting this into (5.17) and expanding for small ε_1 and η yields

$$D_{b0} = D_{b0}^{sf} - K(\varepsilon_2)\varepsilon_1, \quad (5.18)$$

where $K(\varepsilon_2)$ is a smooth function of ε_2 [578]. Assuming smooth dependencies of ε_1 and ε_2 on the system parameter p for $p > p_{sf}$, we see from (5.18) that D_{b0} varies smoothly with p . For instance, suppose ε_1 has a power-law dependence on p : $\varepsilon_1(p) \sim (p - p_{sf})^\gamma$, where $\gamma > 0$. Then this dependence is reflected in $D_{b0}^{sf} - D_{b0} \sim (p - p_{sf})^\gamma$, for $p > p_{sf}$.

5.4.3 A Two-Dimensional Model

The structure of fractal basin boundaries and basin boundary metamorphoses in two dimensions can be understood by constructing invertible-map models based on the horseshoe dynamics [578], such as the one shown schematically in Fig. 5.12. Consider the rectangle ABFE, outside which there are two attractors, denoted by L and R . All initial conditions to the left of the vertical line AB lead to trajectories approaching the attractor L , and all initial conditions to the right of EF go to the attractor R . In ABFE, there are three unstable periodic orbits, denoted by S_1 , S_2 , and S_3 . The action of the dynamics is that of a double horseshoe, i.e., the rectangle is squeezed vertically, stretched horizontally, and placed back into the original rectangular region, forming a double S-shape. As a system parameter p changes from p_1 (Fig. 5.12a) to p_2 (Fig. 5.12b) and to p_3 (Fig. 5.12c), a smooth-to-fractal basin boundary metamorphosis occurs for p_{sf} ($p_1 < p_{sf} < p_2$), and a fractal-to-fractal basin boundary metamorphosis occurs for p_{ff} ($p_2 < p_{ff} < p_3$). Throughout the parameter range, the stable and the unstable manifolds of S_3 cross each other homoclinically. As can be argued below, the smooth-to-fractal boundary metamorphosis at p_{sf} is induced by the homoclinic tangencies between the stable and the unstable manifolds of S_1 , while the fractal-to-fractal boundary metamorphosis is induced by those between the stable manifold of S_2 and the unstable manifold of S_3 .

In Fig. 5.12a, the unstable manifolds of S_2 and S_3 cross the stable manifold of S_3 , so there is a vertical bar UR that maps to the region DR located to the right of the vertical line EF. As a result, all initial conditions in the rectangle CDFE, except for a set of measure zero, map asymptotically to the right of EF and approach the attractor R . We also see that the unstable manifolds of S_1 and S_2 cross the stable manifold of S_2 , and hence the vertical strip VR maps to the region CR to the right of

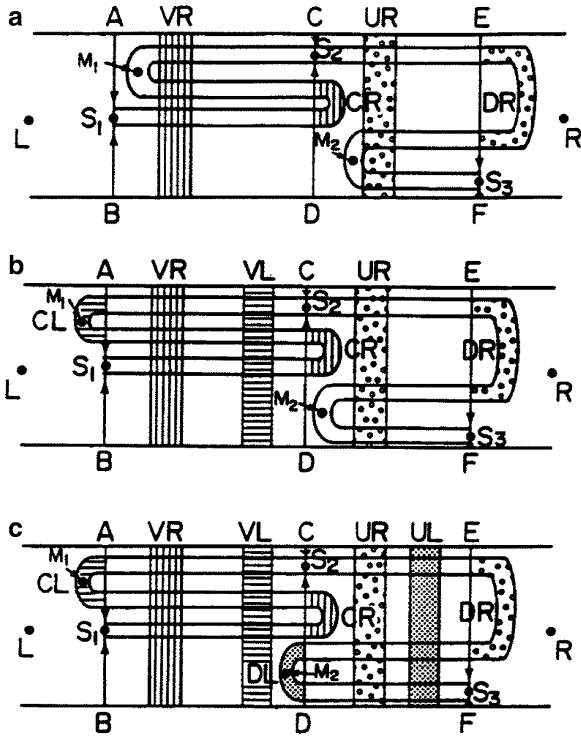


Fig. 5.12 A two-dimensional horseshoe model, where L and R are two attractors, and $S_{1,2,3}$ are saddle points. The double S-shaped band represents the image of rectangle $ABFE$ under the map. (a) For $p = p_1 < p_{sf}$, the vertical line AB is the smooth basin boundary and S_1 is then accessible to the attractor R . (b) For $p_{sf} < p = p_2 < p_{ff}$, the basin boundary consists of a Cantor set of vertical lines in the rectangle $ABDC$ and the accessible orbit to R is replaced by S_2 . (c) For $p = p_3 > p_{ff}$, the basin boundary is a Cantor set of vertical lines in the larger rectangle $ABFE$. In this case, S_2 is no longer accessible to R . The newly accessible orbit on the basin boundary is S_3 [578] (with kind permission from World Scientific Publishing Co.)

the vertical line CD . The consequence is that all initial conditions in $ABDC$, except for a set of measure zero, map to the right of CD . Combining the dynamics on the rectangles $CDFE$ and $ABDC$ so described, we see that all initial conditions in the larger rectangle $ABFE$, except for a set of measure zero, result in trajectories that asymptotically go to the attractor R . In this case $p = p_1 < p_{sf}$, and the boundary between the basins of attraction of L and R is AB , the stable manifold of S_1 , which is smooth. Furthermore, S_1 is an unstable periodic orbit on the basin boundary that is accessible to the attractor R .

For $p = p_{sf}$ (not shown), homoclinic tangencies between the stable and the unstable manifolds of S_1 occur, resulting in subsequent homoclinic crossings for $p > p_{sf}$, as shown in Fig. 5.12b. In this case, the vertical strip VL maps to the region CL to the left of AB and goes to the attractor L . However, the vertical strip VR still maps

to the right of CD, which eventually goes to the attractor R . In ABDC, all initial conditions (except for a set of measure zero) go either to the attractor R or to the attractor L . The vertical strips that approach asymptotically R and L define two horizontal Cantor sets that intertwine in a fractal manner. The basin boundary is thus fractal with a dimension between 1 and 2. Because of the fractal boundary, S_1 is no longer accessible to R for $p > p_{sf}$. The newly accessible periodic orbit to R is S_2 .

As p increases further, we can imagine that for $p_2 < p = p_{ff} < p_3$, the unstable manifold of S_3 becomes heteroclinically tangent to the stable manifold of S_2 (the vertical line CD). As shown in Fig. 5.12c, the subsequent heteroclinic crossings stipulate that the vertical bar UL in CDFE maps to the region DL to the left of CD. As a result, not only a set of vertical strips in ABDC but also such a set in CDFE map to the attractor L . However, there are vertical strips in ABDC and CDFE that map to the attractor R . We see that as p increases through p_{ff} , the fractal basin boundary originally confined to the small rectangle ABDC extends suddenly into the rectangle CDFE, causing a sudden increase in the box-counting dimension of the basin boundary from one fractional value to another between 1 and 2. After the heteroclinic tangencies, S_2 is no longer accessible to the attractor R . For $p > p_{ff}$, the accessible orbit to R on the basin boundary is S_3 .

5.5 Wada Basin Boundaries

Our discussion so far has been restricted to situations in which there are two coexisting basins of attraction. When a dynamical system possesses more than two coexisting attractors, a type of fractal basin boundary, namely Wada basin boundaries [406, 558–561, 613], can arise. For such a case, every boundary point of one basin of attraction is simultaneously a boundary point of the other basins.

To imagine a Wada basin boundary, take the map of the continental United States and consider the boundaries between the states. Almost all boundary points are common to two states, but there are a few dozen of points that are common to three states, and there exists a single boundary point that is shared by four states (the Four-State Corner bordering Arizona, Utah, Colorado, and New Mexico). In the realm of nonlinear dynamical systems, more complicated situations can arise: the set of boundary points that are common to more than two basins of attraction can be fractal. The history and the topology of Wada basins are presented in detail in the review of Aguirre et al. [7].

To give an example, we examine the forced Duffing's oscillator for parameters where on the stroboscopic map, there are two fixed-point attractors, and an attractor at infinity. The basins of attraction of these three attractors are shown in Fig. 5.13 in three different colors. The Wada property of the basin boundaries can be seen, since successive magnifications of any region containing the boundary exhibit all three colors. Another example from the forced damped pendulum is shown in Fig. 5.14.

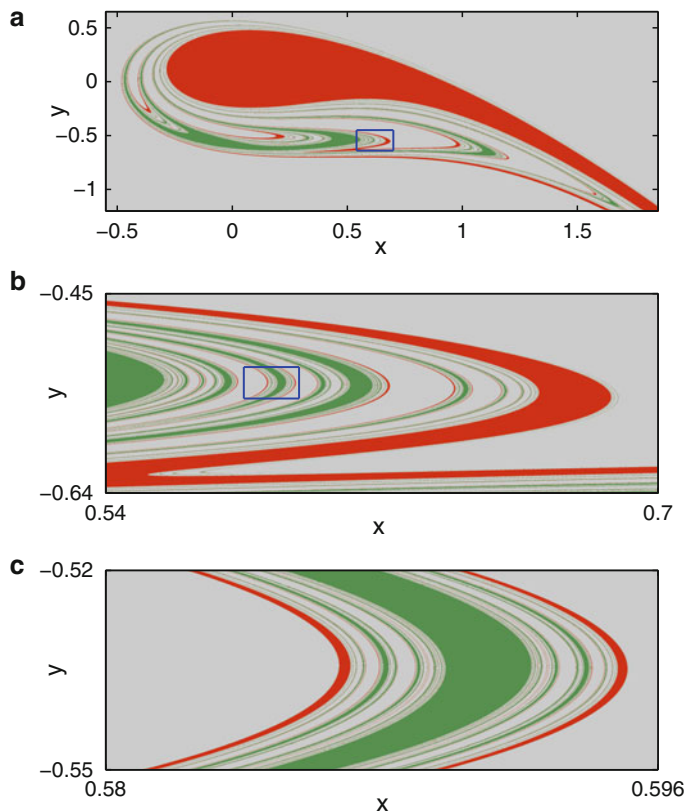


Fig. 5.13 Wada basin boundary for the forced Duffing's oscillator $\ddot{x} + 0.1\dot{x} + x - x^2 = 0.06\sin(0.8t)$ on the stroboscopic section $(x, y \equiv \dot{x})$, where (b) is a magnification of the box in (a), and (c) is the magnification of the box in (b) (Figure by Y. Do.)

For two-dimensional invertible maps, or equivalently, three-dimensional flows, the mechanism for Wada basin boundaries is well understood, due to the work of Kennedy, Nusse, and Yorke [406, 558–561]. In particular, Kennedy and Yorke proved a theorem [406] stating that if \mathbf{p} is a periodic point on the basin boundary, and if the following two conditions are satisfied, (1) its unstable manifold intersects every basin, and (2) its stable manifold is dense in each of the basin boundaries, then the basins have the Wada property. This can be intuitively understood by referring to Fig. 5.15, where there are K coexisting basins, denoted by B_1, B_2, \dots, B_K . Suppose \mathbf{p} is a periodic point on the boundary of B_1 that is accessible to B_1 . Let $W^s(\mathbf{p})$ and $W^u(\mathbf{p})$ be the stable and the unstable manifolds of \mathbf{p} , where $W^s(\mathbf{p})$ is the basin boundary of B_1 . Now arbitrarily choose a point $\mathbf{x} \in W^s(\mathbf{p})$ and imagine a circle $C_\varepsilon(\mathbf{x})$ of radius ε centered at \mathbf{x} . Since $W^u(\mathbf{p})$ intersects every basin, $C_\varepsilon(\mathbf{x})$ must contain points of every basin, which can be seen by considering a one-dimensional curve segment D_k in the basin B_k that intersects $W^u(\mathbf{p})$, for $k = 1, \dots, K$. Under inverse iterations of the map, the images of the curves will be arbitrarily close to

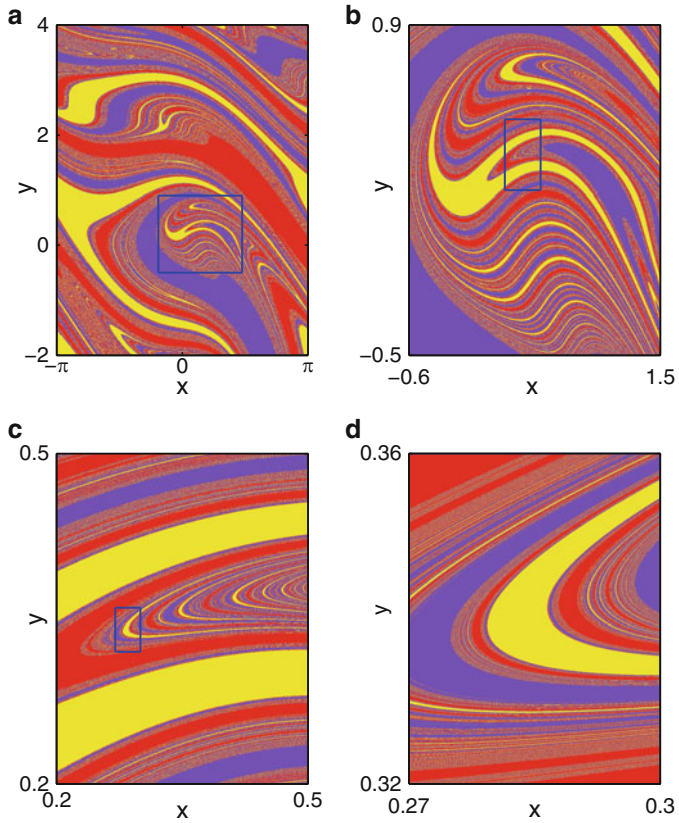


Fig. 5.14 Wada basin boundary for the forced damped pendulum $\gamma = 0.2, f_0 = 1.66$ in (5.2), on the stroboscopic section $(x, y \equiv \dot{x})$. At these parameters, three attracting limit cycles coexist. Panels (b, c, d) are successive magnifications of boxes in (a, b, c), respectively (Figure by Y. Do)

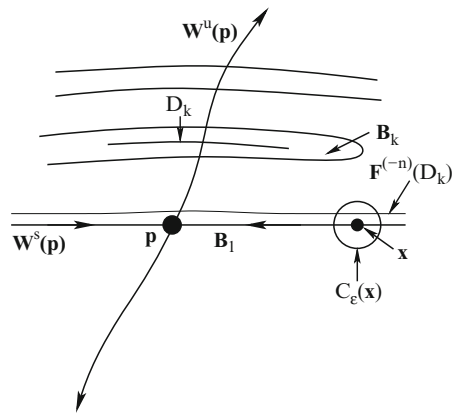


Fig. 5.15 Schematic illustration of the setting for establishing the Wada property. See text for details

the stable manifold of \mathbf{p} and therefore be in $C_\epsilon(\mathbf{x})$ [547]. Thus, the boundary of B_1 must be the boundaries of all other basins. Since $W^s(\mathbf{p})$ is dense in each of the basin boundaries, all boundaries are common to all basins, and hence the Wada property is fulfilled.

Computationally, to verify condition (1), one can plot a piece of the unstable manifold, trace it under the dynamics, and determine whether it intersects all basins of interest. Condition (2) is more difficult to verify from numerical traces of the stable manifold. To overcome these difficulties, Nusse and Yorke proposed the construction of *basin cells*, which leads to numerically verifiable conditions guaranteeing that the boundary of a basin is a Wada basin boundary [559, 560].

To explain the idea of basin cells, consider an invertible dissipative map \mathbf{f} in the plane. Traditionally, the basin of attraction of an attractor is defined to be the set of points that approach the attractor asymptotically. Since there has been no rigorous way to determine whether an attractor is chaotic or whether there are multiple coexisting attractors, this concept of “basin” is in principle ill defined. Nusse and Yorke redefined a “basin” as the set of points that enter a trapping region [559, 560]. A compact region Q is a *trapping region* if $\mathbf{f}(Q) \in Q$ and $\mathbf{f}(Q) \neq Q$. These two conditions guarantee that a trajectory entering a trapping region does not leave the region, and there must then be at least one attractor inside. The basin of the trapping region Q is the set of points that map into the interior of Q . A trapping region may contain invariant sets such as chaotic saddles; that is, there can be points in the region whose trajectories do not converge to an attractor. Trapping regions of practical importance are those having piecewise smooth boundaries that consist of finitely many smooth curve segments. If a trapping region Q is constructed such that (1) there is an unstable periodic orbit on its boundary and (2) the boundary consists of pieces of the stable and the unstable manifolds of the periodic orbit, then Q is a *basin cell*. Although there is an infinite number of unstable periodic orbits on a fractal basin boundary, only a few may be “qualified” to generate a basin cell. Thus, in order to have a basin cell, the unstable periodic orbit on the cell boundary needs to be chosen carefully [559, 560].

Figure 5.16 illustrates two types of basin cells that are topologically equivalent to some basin cells that can be explicitly constructed from the system of forced damped pendulum in parameter regions with Wada basin boundaries shown in Fig. 5.14a–d. Let \mathbf{P} denote the unstable periodic orbit that generates a basin cell C_P . As shown in Fig. 5.16, for a periodic point \mathbf{p} of \mathbf{P} , its unstable manifold can form an *arc* that starts from \mathbf{p} and ends at a corner point, an intersection point between the stable and the unstable manifolds of \mathbf{p} . Such an arc is outside the basin cell (except the endpoints). The union of all supporting arcs, one for each periodic point \mathbf{p} of \mathbf{P} , is called the *scaffolding* of the basin cell C_P [559, 560]. For instance, for the cell in Fig. 5.16a, the scaffolding consists of the union of two supporting arcs, while in Fig. 5.16b, the scaffolding is the union of three supporting arcs. With such a geometric construction, Nusse and Yorke proved the result that if the scaffolding of C_P intersects at least two other basins, the boundary of the basin cell C_P is a Wada basin boundary. This result is remarkable because all the quantities and conditions

indicates that in a situation in which random perturbations or computational errors are present, as μ adiabatically increases through μ_0 , it is fundamentally impossible to determine where an orbit placed on the node (attractor) for $\mu_0 - \varepsilon_1 < \mu < \mu_0$ would go.

5.6 Sporadically Fractal Basin Boundaries

Sporadically fractal basin boundaries have the character of a bounded curve, say $y = g(x)$, such that $g(x)$ is a differentiable (or smooth) function except for a set of x values of zero measure. Furthermore, the nondifferentiable set of x values is a fractal set with dimension less than one. The curve thus has a dimension between one and two. This type of basin boundary was discovered by Rosa et al. [651, 652] and was subsequently analyzed rigorously by Hunt et al. [346]. It was conjectured that sporadically fractal basin boundaries exist in typical dynamical systems of phase-space dimension at least two for noninvertible maps, at least three for invertible maps (thus at least four for flows).

In order to highlight the relevance of sporadically fractal basin boundaries to physical situations, in what follows we describe the occurrence of this type of boundary in the context of chaotic phase synchronization in systems described by differential equations. We then discuss a mathematical model to understand the dynamical origin and properties of these exotic basin boundaries.

5.6.1 Chaotic Phase Synchronization

Chaotic phase synchronization was discovered by Rosenblum, Pikovsky, and Kurths in 1996 [653] and has since become an active area of research (see [80, 602]). If one examines a chaotic attractor from a three-dimensional flow, such as the Rössler oscillator, one finds that trajectories on the attractor exhibit rotation-like motions around the z -axis, as shown in Fig. 5.17. The motions have a well-defined center of rotation and a unique direction (counterclockwise in Fig. 5.17b). Using the center of rotation and an arbitrary reference line, a rotational angle ϕ can be defined, as shown schematically in Fig. 5.18.

For the Rössler attractor in Fig. 5.17, it is convenient to use cylindrical coordinates: $(x, y, z) \rightarrow (r, \phi, z)$, where $r = \sqrt{x^2 + y^2}$ and $\phi = \tan^{-1}(y/x)$ (within one rotation). For a chaotic trajectory, from a reference point corresponding to the initial condition, the phase variable $\phi(t)$ is a monotonically increasing function of t . In cylindrical coordinates, the Rössler equations can be conveniently written as $d\mathbf{x}/dt = \mathbf{R}(\mathbf{x})$, where $\mathbf{x} \equiv (r, \phi, z)$. The question Rosa et al. asked [652] was whether the phase variable can be locked with respect to an external periodic driving. One can imagine that if the periodic driving is weak, the phase will be chaotic, but under strong driving, it is likely that the chaotic rotation would follow more or less that of the external periodic pattern. In this case the phase variable of the chaotic oscillator

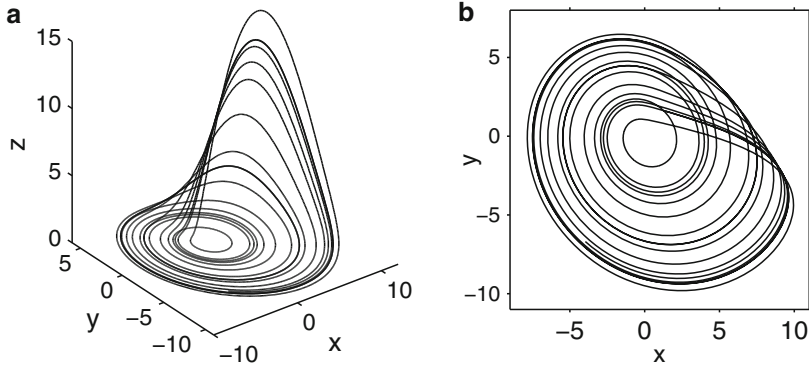
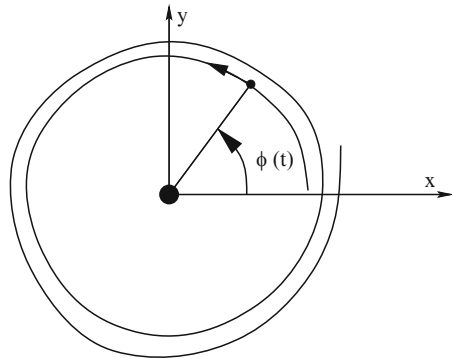


Fig. 5.17 (a) Chaotic attractor from the Rössler oscillator: $\dot{x} = -(y + z)$, $\dot{y} = x + 0.25y$, and $\dot{z} = 0.9 + z(x - 6.0)$, in the three-dimensional phase space. (b) Projection of the attractor on the (x, y) -plane. A chaotic trajectory exhibits a rotation-like motion

Fig. 5.18 Definition of phase variable ϕ for a chaotic rotation



is said to have been synchronized (paced) with the phase of the external periodic signal. To address this question, consider the following general system:

$$\frac{d\mathbf{x}}{dt} = S(\mathbf{x}, s)\mathbf{R}(\mathbf{x}) + A\mathbf{P}(t), \tag{5.19}$$

where $S(\mathbf{x}, s) = 1 + s(r^2 - \bar{r}^2)$, $\mathbf{P}(t) = [0, \sin(2\pi t/T), 0]$, s and \bar{r} are parameters of the modulating function $S(\mathbf{x}, s)$ (\bar{r} can be chosen to be the average value of $r(t)$ for $s = 0$ and $A = 0$), and A is the amplitude of the external periodic driving. To search for synchronization, it is convenient to use $\theta = \phi(t) - 2\pi t/T$, the phase difference between the chaotic oscillator and the external periodic signal. Phase synchronization is defined by the locking of θ within 2π : $-\pi < \theta < \pi$. For a given T , phase synchronization was found to occur for sufficiently large values of A [652]. In fact, there is a region of finite area in the two-dimensional parameter space (T, A) in which phase synchronization occurs. To understand the fundamental dynamical mechanism for the synchronization, Rosa et al. suggested to define the angle variable θ on the

real line, $-\infty < \theta < +\infty$, rather than on the circle, $-\pi \leq \theta \leq \pi$. The angle thus becomes *lifted*. The phase-synchronized state corresponds to an attractor confined within $-\pi < \theta < \pi$. The attractor is chaotic because the amplitude dynamics remains chaotic even when its phase is locked. Due to the invariance of the system under the transformation $\theta \rightarrow \theta \pm 2\pi$, there is an infinite array of such attractors spaced by 2π in θ .

Imagine for a fixed T , as A increases through a critical value A_c , phase synchronization occurs so that for $A > A_c$, an infinite array of attractors is formed. For $A < A_c$, there is no phase locking so that θ cannot be confined in any of the 2π intervals. A trajectory can thus move across the entire θ -axis. However, for A slightly below A_c , the trajectories will be confined within one of the 2π intervals for long time before moving to an adjacent 2π interval. There is thus *transient chaos* corresponding to the temporal phase locking. The time it takes for a trajectory to escape an attractor and to move to an adjacent one is typically much smaller than the time that the trajectory stays on the attractor. What can be expected is thus the confinements of θ values within 2π for long stretches of time and rapid jumps of magnitude 2π amid the long confinements. This 2π -jump phenomenon has indeed been observed numerically and experimentally [80]. The point is that the transition to chaotic phase synchronization can be regarded as crisis-like transition whereby isolated chaotic attractors are formed from transient chaos.

Rosa et al. found that after the onset of phase synchronization, the basin boundaries between the chaotic attractors in two adjacent 2π cells are sporadically fractal. The boundaries are in fact similar to those from the two-dimensional map (5.5), as shown in Fig. 5.4.

5.6.2 Dynamical Mechanism

To understand how sporadically fractal basin boundaries can arise in dynamical systems, Hunt et al. [346] proposed a class of two-dimensional maps (5.5), where the x -dynamics is governed by the following one-dimensional map:

$$f(x) = \begin{cases} 9x/(4-5x), & \text{for } x \leq 0, \\ 9x/4, & \text{for } 0 \leq x \leq 4/9, \\ (81/4)(x-x^2), & \text{for } 4/9 \leq x \leq 5/9, \\ (9/4)(1-x), & \text{for } x \geq 5/9, \end{cases} \quad (5.20)$$

as shown in Fig. 5.19.

This map has two invariant sets: a stable fixed-point attractor at $x = -1$ with a negative Lyapunov exponent and a “middle ninth” Cantor set in $0 \leq x \leq 1$, the set of initial conditions in the unit interval that do not approach the attractor. The Cantor set is in fact a repeller with a positive Lyapunov exponent $\ln(9/4)$ because the

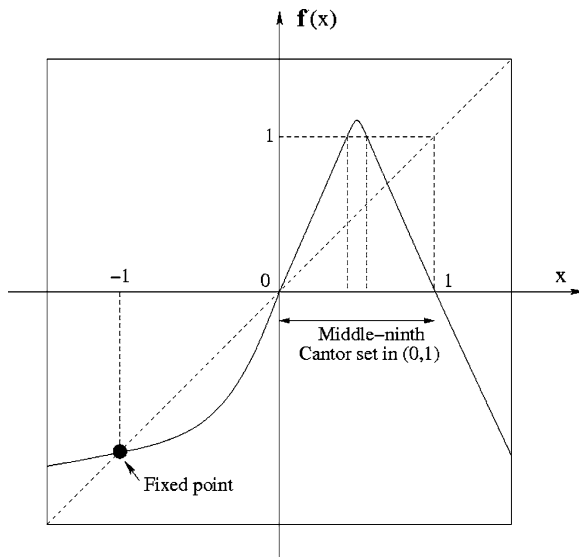


Fig. 5.19 One-dimensional map (5.20) as $f(x)$ in (5.5)

slopes of the map about the Cantor set are $\pm 9/4$. For the two-dimensional map (5.5), at each iterate every vertical line segment is expanded by the factor $\lambda > 1$. Thus almost all initial conditions approach asymptotically either $y = +\infty$ or $y = -\infty$, which can be regarded as the two attractors of the system. The boundary between the two basins of attraction is a function $y = g(x)$, the dynamics on which are determined by $f(x)$. Since $f(x)$ has two invariant sets and since the y -dynamics is unstable, on the basin boundary there are two invariant sets as well: a saddle point (at $x = -1$) with one positive and one negative Lyapunov exponent, and a chaotic repeller with two positive Lyapunov exponents. Numerical experiments revealed that $g(x)$ is smooth for almost all x values but nondifferentiable for a set of x values constituting the middle-ninth Cantor set in the one-dimensional map $f(x)$. The box-counting dimension of the curve $y = g(x)$ turns out for $\lambda = 1.1$ to be $D_{b0} \approx 1.75$ [346].

How is it that the basin boundary curve can be smooth at all x except for a set of measure zero, yet has a box-counting dimension greater than 1? To understand this property, Hunt et al. [346] considered the Hölder exponent $H(x)$ at x of the function $g(x)$: $|\Delta y| \sim |\Delta x|^{H(x)}$, where Δx is infinitesimal and $\Delta y = g(x + \Delta x) - g(x)$. If $H(x) < 1$, $g(x)$ is not differentiable at x , but if $g(x)$ is differentiable at x , then $H(x) = 1$. Points on $y = g(x)$ with $H(x) < 1$ exhibit a cusplike, spiked behavior. Now consider two nearby points (x_0, y_0) and $(x_0 + \Delta x_0, y_0 + \Delta y_0)$ on the basin boundary and iterate them n times under the map (5.5). Since they are on the basin boundary, their images (x_n, y_n) and $(x_n + \Delta x_n, y_n + \Delta y_n)$ must also be on the basin boundary. For n not too large, Δx_n and Δy_n can still be regarded as small quantities. Since the n th iterate of the map (5.5) provides a smooth transformation of the neighborhood of (x_0, y_0) to the neighborhood of (x_n, y_n) , the Hölder exponents are

the same for (x_0, y_0) and (x_n, y_n) : $|\Delta y_0| \sim |\Delta x_0|^H$ and $|\Delta y_n| \sim |\Delta x_n|^H$. From (5.5), we have $\Delta x_n \sim \exp(\lambda_1 n) \Delta x_0$, where λ_1 is the Lyapunov exponent of the one-dimensional map $f(x)$. If $H < 1$, $|\Delta y|$ is much greater than $|\Delta x|$, so the effect of Δx on the y -dynamics is negligible. We have $\Delta y_n \sim \exp(\lambda_2 n) \Delta y_0$, where $\lambda_2 = \ln \lambda$. The Hölder exponent is thus given by $H = \lambda_2 / \lambda_1$ if $\lambda_1 > \lambda_2$. Otherwise, we have $H = 1$ because the assumption $H < 1$ is contradicted. Since there are two possible values for the Lyapunov exponent λ_1 in the one-dimensional map $f(x)$ (corresponding to the two invariant sets), and particularly $\lambda_1 = \ln(9/4)$ for trajectories on the middle-ninth Cantor set, we see that $H < 1$ if $\lambda < 9/4$. For randomly chosen x on the basin boundary (with Lebesgue measure one), the trajectory goes to the attractor at $x = -1$ that has $\lambda_1 < 0$. For these points $H = 1$, and the boundary is smooth.

The relationship between the Hölder exponent and the Lyapunov exponents can be used to obtain the box-counting dimension of the basin boundary curve $y = g(x)$. Suppose we cover the (x, y) -plane with square boxes of linear size $\varepsilon \ll 1$. If the boundary curve contained in a column of width ε is smooth, i.e., no points of the middle-ninth Cantor set lie in it ($H = 1$), the number of boxes required to cover the curve segment is of order 1. If the boundary curve in a column of boxes contains points of the Cantor set so that $H < 1$, the variation of the curve in the y -direction is $|\Delta y| \sim \varepsilon^H$ (because $\Delta x = \varepsilon$). The number of boxes required to cover the boundary curve in this column is thus of order $\varepsilon^H / \varepsilon = \varepsilon^{H-1}$. Since the total number of boxes needed to cover the Cantor set (the chaotic repeller of $f(x)$) of dimension D_x is ε^{-D_x} , the number of boxes necessary to cover the spiked parts of the basin boundary curve is $\varepsilon^{-(1+D_x-H)}$. This implies that the box-counting dimension of the chaotic repeller embedded in the basin boundary is $D_0 = 1 + D_x - H$. Taking into account the fact that the number of boxes required to cover the smooth parts of the boundary is of order ε^{-1} , we see that if $1 + D_x - H < 1$, then ε^{-1} is much greater than $\varepsilon^{-(1+D_x-H)}$, so in this case the number of boxes needed to cover the whole boundary curve is of order ε^{-1} . Conversely, this number is of order $\varepsilon^{-(1+D_x-H)}$ if $1 + D_x - H > 1$. These estimates yield the box-counting dimension of the boundary curve $y = g(x)$ as

$$D_{b0} = \max\{1, 1 + D_x - H\}. \quad (5.21)$$

An interesting observation is that the basin boundary's being spiky, i.e., $H < 1$, is not sufficient to make $D_{b0} > 1$, i.e., to make the boundary sporadically fractal. To have $D_{b0} > 1$ requires $H < D_x$, i.e., that the dimension D_0 of the repeller be larger than 1. This means that the spiked behavior should be sufficiently intense for sporadically fractal boundaries to arise. The uncertainty exponent is thus

$$\alpha = 2 - D_{b0} = 1 - D_x + H = 2 - D_0 < 1. \quad (5.22)$$

For the model described by (5.5) and (5.20), we have $D_x = \ln 2 / \ln(9/4)$ and $H = \ln \lambda / \ln(9/4)$, so $D_{b0} = D_0 = 2 - \alpha = 1 + \ln(2/\lambda) / \ln(9/4) > 1$ for $\lambda < 2$ and $D_{b0} = \alpha = 1, D_0 < 1$, for $\lambda > 2$.

5.7 Riddled Basins

We have seen up to now several types of complicated basins. Despite differences, a common feature among them is open sets (volumes) contained in a basin. In this section we discuss riddled basins, basins that do not contain any open sets but nonetheless have a positive Lebesgue measure. Because a riddled basin has no open sets, for every initial condition that approaches the attractor with a riddled basin asymptotically, there are initial conditions *arbitrarily nearby* that go to another coexisting attractor. Thus, an arbitrarily small uncertainty in the initial condition can lead to a completely different attractor. Riddled basins are therefore space-filling. In a D -dimensional phase space, $D_{b0} = D$, riddled basins are *fat fractals* [234, 564, 773]. In fact, the uncertainty exponent associated with a riddled basin is close to zero, which means that a vast reduction in the error in specifying the initial conditions results in hardly any improvement in one's ability to predict the final attractor. As a consequence, prediction of attractors for specific initial conditions and parameters becomes practically impossible. Because of this serious consequence, there has been much effort devoted to riddled basins (for a review and historical comments, see [7]).

The dynamical conditions for riddling to occur were first described by Alexander et al. [11]. They offered the following definition for a riddled basin: *The basin of attraction of an attractor is riddled if its complement intersects every disk in a set of positive measure.* Roughly, the term “disk” here refers to D -dimensional phase-space volumes of all sizes. In order to argue that the basin of a chaotic attractor is riddled, the following two conditions need to be established: (1) a set of positive measure is attracted to the attractor; and (2) sufficiently many points near the attractor are repelled from it. In particular, to prove condition (1), one can compute the transverse Lyapunov exponent (to be defined below) and show that it is negative [11]. To prove condition (2), it is necessary to show that there exists an open *dense* set near the attractor where points approach another coexisting attractor. In contrast, a fractal basin is open and it is defined with respect to the basin boundary: a basin is fractal if its boundary is a fractal set. The mathematical feature that distinguishes a riddled basin from a fractal one is then that the former is a closed set of positive measure, while the latter is open.

A necessary condition for riddling is the existence of an *invariant subspace*, which often results from a symmetry of the system. An example is the following system of N coupled chaotic oscillators:

$$\frac{d\mathbf{x}_i}{dt} = \mathbf{F}_i(\mathbf{x}_i) + K \sum_j \mathbf{H}(\mathbf{x}_i - \mathbf{x}_j), \quad i = 1, \dots, N, \quad (5.23)$$

where $\mathbf{F}_i(\mathbf{x}_i)$ is the velocity of oscillator i when uncoupled, and the coupling is represented by strength K and the function $\mathbf{H}(\mathbf{x}_i - \mathbf{x}_j)$ that satisfies the condition $\mathbf{H}(\mathbf{0}) = \mathbf{0}$. When the individual oscillators are identical, i.e., $\mathbf{F}_i = \mathbf{F}_j$, the

synchronous state $\mathbf{x}_i(t) = \mathbf{x}_j(t)$ ($i, j = 1, \dots, N$) is a solution to (5.23). In this case, the dynamical equations are identical for each oscillator, so oscillators starting synchronized remain so forever. The subspace defined by $\mathbf{x}_i(t) = \mathbf{x}_j(t)$ ($i, j = 1, \dots, N$) is therefore invariant. The existence of such an invariant subspace was the starting point for analyzing the dynamics of coupled chaotic oscillators in most existing works in the area of chaotic synchronization [602, 711]. In fact, the first experimental evidence for riddled basins was found in this context (see Fig. 1.18).

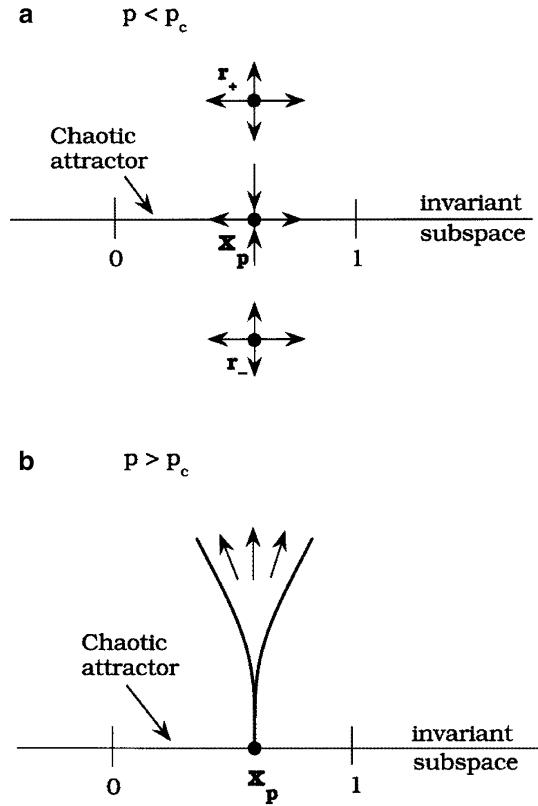
5.7.1 Riddling Bifurcation

How does a riddling bifurcation occur that creates a riddled basin? The answer was provided in [455]. In a two-dimensional phase space, the invariant subspace is a line. In this case, the onset of riddling is determined by a saddle-repeller bifurcation [294, 295]. In particular, the chaotic attractor \mathcal{A} in the invariant subspace is one-dimensional. Before the bifurcation, \mathcal{A} attracts all points in some neighborhood of itself, and all the periodic orbits embedded in the chaotic attractor are saddles in the full phase space. At the riddling bifurcation, one of the periodic orbits, usually of low period, becomes transversely unstable. Since this periodic orbit is already unstable in the attractor, it becomes a repeller in the two-dimensional phase space. To be concrete, let \mathbf{x}_p be an unstable fixed point embedded in the chaotic attractor in the invariant subspace. The point is stable transversely to this subspace for $p < p_c$, as shown in Fig. 5.20a. Riddling occurs when \mathbf{x}_p loses its transverse stability as a parameter p passes through a critical value p_c . For such systems, the loss of transverse stability is induced by the collision at $p = p_c$ of two point repellers \mathbf{r}_+ and \mathbf{r}_- , located symmetrically with respect to the invariant subspace, with the saddle at \mathbf{x}_p (a saddle-repeller bifurcation). These two repellers exist only for $p \leq p_c$, as shown in Fig. 5.20a. For $p > p_c$, the saddle \mathbf{x}_p becomes a repeller, and the two repellers \mathbf{r}_+ and \mathbf{r}_- off the invariant subspace no longer exist.

Due to nonlinearity, a “tongue” opens at \mathbf{x}_p , allowing trajectories near the invariant subspace to escape for $p > p_c$, as shown in Fig. 5.20b. Each preimage of \mathbf{x}_p also develops a tongue simultaneously. Since preimages of \mathbf{x}_p are dense in the invariant subspace, an infinite number of tongues open up simultaneously at $p = p_c$, indicating that initial conditions arbitrarily close to the invariant subspace can go to another attractor.

At the riddling bifurcation a single periodic orbit becomes transversally unstable. As the parameter p is increased further, more and more periodic orbits become unstable until, for another critical parameter $p_c^0 (> p_c)$, the full attractor in the invariant subspace becomes transversely unstable. This occurs when the average transverse Lyapunov exponent λ_T becomes positive. This bifurcation is called the *blowout bifurcation* [30, 435, 727].

Fig. 5.20 Riddling bifurcation at p_c . **(a)** Unstable saddle fixed point in the invariant subspace and two repellers off the invariant subspace for $p < p_c$ (before the saddle-repeller bifurcation). **(b)** Tongue structure formed for $p > p_c$, after the onset of riddling. Trajectories originated from initial conditions inside the tongues escape the invariant subspace to $+\infty$ [455] (Copyright 1996, the American Physical Society)



5.7.2 An Example

To make these ideas more concrete, we use the following map [455]:

$$x_{n+1} = 4x_n(1 - x_n), \tag{5.24}$$

$$y_{n+1} = pe^{-b(x_n - x_p)^2} y_n + y_n^3,$$

where $y = 0$ defines the invariant subspace as a trajectory with $y_0 = 0$ will have $y_n = 0$ and $b > 0$ is a parameter. In this system, \mathcal{A} is the fully developed chaotic attractor of the logistic map, and $x_p = 3/4$ denotes the nontrivial unstable fixed point of the logistic map.

The two eigenvalues of the unstable fixed point $\mathbf{x}_p = (x_p = 3/4, y = 0)$ are $(\Lambda_x, \Lambda_y) = (-2, p)$. Thus, \mathbf{x}_p is stable in the y direction for $p < 1$ and unstable for $p > 1$. This fixed point is a saddle for $p < 1$. For $p < 1$, there are two other unstable fixed points located at $\mathbf{r}_\pm \equiv (x_p, \pm\sqrt{1-p})$, which have eigenvalues $(-2, 3-2p)$, both being repellers for $p < 1$, as shown in Fig. 5.20a. The repellers collide with each other and with the saddle at $p = p_c = 1$ in a saddle-repeller bifurcation, and

they do not exist for $p > 1$. Thus, beyond the riddling bifurcation (for $p > 1$), two tongues, symmetrically located with respect to the invariant subspace, open up at $x = x_p$, allowing trajectories near $y = 0$ to escape to $|y| = \infty$. Observe that the cubic term in the y -dynamics guarantees that if $|y_n| > 1$, then $|y_{n+1}| > |y_n| > 1$. Once a trajectory reaches $|y| = 1$, its y value tends to infinity rapidly. As a result, $y = \pm\infty$ can be regarded as coexisting attractors, A_{\pm} , of (5.24) with \mathcal{A} , fulfilling the condition for riddling.

The transverse Lyapunov exponent is the average of the logarithms of the stretching rates of the y -dynamics at $y = 0$ along a trajectory of the x -dynamics. That is,

$$\lambda_T = \left\langle \ln \left| \frac{dy_{n+1}}{dy_n} \right| \right\rangle_{|y=0}, \quad (5.25)$$

where the angled brackets denote an average taken with respect to the natural measure of the attractor \mathcal{A} . Since $dy_{n+1}/dy_n = p \exp[-b(x_n - x_p)^2]$ at $y = 0$, we have $\lambda_T = \ln p - b(\langle x^2 \rangle - 2\langle x \rangle x_p + x_p^2)$. Substituting the averages for the chaotic attractor of the x -dynamics, we obtain

$$\lambda_T = \ln p - 3b/16. \quad (5.26)$$

The blowout bifurcation takes place at $p_c^0 = \exp(3b/16) > 1$.

5.7.3 Scaling Relation

A quantity characterizing the degree of riddling of a basin is the ratio between the sizes of the basins of the attractors A_+ (or A_-) and \mathcal{A} , which can be computed as follows. Take a line parallel to the invariant subspace at distance $y_0 \ll 1$ and determine the fraction $F(y_0)$ of the length of this line in the basin of A_+ (or A_-). The fraction typically obeys the following scaling law [567]:

$$F(y_0) \sim |y_0|^\eta, \quad (5.27)$$

where η is a positive exponent. As $y_0 \rightarrow 0$, the fraction of the basin of A_{\pm} approaches zero, but for any finite $|y_0|$ this fraction is nonzero. For p values close to the blowout bifurcation point p_c^0 , a stochastic model by Ott et al. [567] predicts the exponent η to be

$$\eta = \frac{|\lambda_T|}{Q}, \quad (5.28)$$

where Q represents the diffusion coefficient characterizing the variance of the finite-time transverse Lyapunov exponents (the analogue of Q_2 introduced in Sect. 2.2.2 and in Appendix A). Close to but below the blowout bifurcation point, λ_T is negative and small.

Another measurable quantity is the uncertainty exponent α , defined by $f(\varepsilon) \sim \varepsilon^\alpha$, where $f(\varepsilon)$ is the probability of finding two points within distance ε along a line at distance y_0 from the invariant plane, which belong to different basins

(to those of \mathcal{A} and of A_+ (or A_-)). The stochastic theory predicts, for p close to p_c^0 , that

$$\alpha = \frac{\lambda_T^2}{4Q\lambda_1}, \tag{5.29}$$

where λ_1 is the Lyapunov exponent of attractor \mathcal{A} . Since λ_T is small, the uncertainty exponent is small, signifying a fundamental obstacle to prediction. Due to the fractal nature of the boundary (5.12) does not hold. In this case, we have $D_{b0} = D$ but $\alpha \neq 0$.

5.8 Catastrophic Bifurcation of a Riddled Basin

While symmetry and invariance are common in mathematical models of physical systems, the notion of symmetry and invariance is *nongeneric*, because in physical reality, imperfections or perturbations that destroy system symmetry are always present. In the coupled-oscillator system (5.23), a typical type of imperfection is parameter mismatches among oscillators. The presence of heterogeneity among the vector fields \mathbf{F}_i , no matter how small, immediately destroys the originally invariant subspace defined by the synchronous state. A key question is thus, can a riddled basin be physically observed? Investigation along this line [438, 441] has indicated that riddling is typically destroyed by symmetry-breaking perturbations and is converted into a fractal basin, no matter how small the perturbations are. This has been called *catastrophe of riddling* [438]. However, for small perturbations, the resulting fractal basin may appear similar to a riddled one.

5.8.1 An Example

We consider the following noninvertible two-dimensional map [441]:

$$x_{n+1} = T(x_n) = \begin{cases} 2x_n, & 0 \leq x < 1/2, \\ 2(1-x_n), & 1/2 \leq x \leq 1, \end{cases} \tag{5.30}$$

$$y_{n+1} = f(x_n, y_n) = \begin{cases} px_n y_n + \varepsilon, & |y| < 1 \\ \lambda y_n, & |y| \geq 1, \end{cases}$$

where $T(x)$ is the tent map, p and $\lambda > 1$ are parameters, and ε is the symmetry-breaking parameter. The phase-space region of interest is $\{0 \leq x \leq 1, -\infty < y < \infty\}$. For $\varepsilon = 0$, the system possesses a one-dimensional invariant subspace $y = 0$, which is caused by the reflection symmetry $y \rightarrow -y$. Because $\lambda > 1$, the map has two other attractors: A_{\pm} at $y = \pm\infty$. The chaotic attractor \mathcal{A} of the tent map in $y = 0$ can be the

third attractor of the full system if it is transversely stable. Since $dy_{n+1}/dy_n = px_n$ at $y = 0$, we have $\lambda_T = \ln p + \langle \ln x \rangle = \ln p - 1$. A blowout bifurcation occurs at $p_c^0 = e$.

As ε is increased from zero, no matter how little, the chaotic attractor of the tent map is no longer an attractor of the whole system. A catastrophe of riddling occurs for $p < p_c^0$ as $|\varepsilon|$ is increased from zero, in which the riddled basin of \mathcal{A} for $\varepsilon = 0$ is replaced by the fractal basin either of A_+ or of A_- , depending on the sign of ε . For $p > p_c^0$, the basins of the $y = \pm\infty$ attractors are $y > 0$ and $y < 0$, respectively if $\varepsilon = 0$. In this case, as $|\varepsilon|$ is increased from zero, a smooth-to-fractal basin boundary metamorphosis occurs because the two simple basins ($y > 0$ and $y < 0$) are replaced by fractal ones. Because of the simplicity of (5.30), these bifurcations can in fact be understood analytically to a certain extent.

The replacement of the riddled basin by a fractal one in the presence of a symmetry-breaking perturbation can be seen qualitatively as follows. As discussed above, for $\varepsilon = 0$, the basin of the chaotic attractor \mathcal{A} is a closed set with positive measure, which is the complement of two symmetric open dense sets belonging to the attractors A_{\pm} , respectively. While initial conditions with $y_0 > 0$ or $y_0 < 0$ can go to \mathcal{A} , they cannot cross the invariant line $y = 0$. For $\varepsilon \neq 0$, the dense set of unstable periodic orbits originally embedded in \mathcal{A} in $y = 0$ spread out in the vicinity of $y = 0$, converting \mathcal{A} into a nonattracting chaotic set. Because of this spread of unstable periodic orbits, a trajectory initiated in $y > 0$ can penetrate the originally invariant line $y = 0$ and go to the $y = -\infty$ attractor, and vice versa. The basin of the $y = -\infty$ attractor in $y > 0$ must be open and therefore is fractal.³ The same holds for the basin of the $y = +\infty$ attractor in $y < 0$. Thus, as soon as ε becomes nonzero, the riddled basin of \mathcal{A} is destroyed, and simultaneously, two fractal basins arise. In what follows we analyze how unstable periodic orbits embedded in the original chaotic attractor in \mathcal{A} are perturbed by the symmetry-breaking, based on which we can establish the existence of open, but not dense, sets that belong to the basins of the attractors at infinities.

For concreteness, we consider the map (5.30) with $\varepsilon < 0$ around the blowout bifurcation, i.e., for p less than but close to p_c^0 . Since unstable periodic orbits are structurally stable, we expect that they shift to a small neighborhood about the originally invariant subspace $y = 0$ for $\varepsilon \neq 0$. For example, the original fixed point $\mathbf{x}_p = (x_p, 0)$ (a repeller with an unstable direction in both x and y , where $x_p = 2/3$ is the nontrivial unstable fixed point of the tent map) is shifted to (x_p, y_p) , where y_p is

$$y_p = \frac{-|\varepsilon|}{1 - px_p}. \quad (5.31)$$

³ Consider an open neighborhood \mathcal{B} of one of the attractors at infinity. Choose a point p in its basin and evolve it forward in time. Eventually, the resulting trajectory will approach the attractor, which means that at some finite time, the trajectory will enter \mathcal{B} , say at point p' . The point p' in \mathcal{B} must then have an open neighborhood. Since p' is iterated from p in finite time, p must also have an open neighborhood in the basin.

For $p \approx p_c^0$, we have $px_p \approx 2e/3 > 1$ and hence $y_p > 0$. The eigenvalues of the perturbed fixed point (x_p, y_p) are $\Lambda_x = -2$ and $\Lambda_y = px_p > 1$. Thus, under the symmetry-breaking perturbation, the shifted fixed point is still a repeller. Consider now the period-2 orbit of the tent map: $(x_1^{(2)} = 2/5, 0)$ and $(x_2^{(2)} = 4/5, 0)$. The eigenvalues of the twice iterated map at these points are $\Lambda_x = -4$ and $\Lambda_y = p^2 x_1^{(2)} x_2^{(2)}$. The latter is smaller than unity for $p < 1.77$. The two-cycle is then a saddle in the full phase space. For $\varepsilon \neq 0$, the y -coordinates of the orbit become

$$y_1^{(2)} = \frac{-|\varepsilon|(px_2^{(2)} + 1)}{1 - p^2 x_1^{(2)} x_2^{(2)}} \quad \text{and} \quad y_2^{(2)} = \frac{-|\varepsilon|(px_1^{(2)} + 1)}{1 - p^2 x_1^{(2)} x_2^{(2)}}.$$

Altogether, we observe that (1) an orbit is shifted upward (downward) from $y = 0$ if it is a repeller (saddle), and (2) the eigenvalues of the orbit remain unchanged. In general, this is valid for any periodic orbit. Since all repellers are located in $y > 0$, a trajectory starting in $y < 0$ cannot cross $y = 0$, but since all saddles are located in $y < 0$, a trajectory starting in $y > 0$ can move across the x -axis and go to the $y = -\infty$ attractor. Thus, due to the symmetry-breaking, the $y = -\infty$ attractor acquires a basin in $y > 0$.

The picture depicted above, i.e., saddles shifted downward and repellers upward, is specific to the system (5.30) for the case of $\varepsilon < 0$. For $\varepsilon > 0$, saddles will shift upward and repellers downward. In general, in two dimensions we expect to observe saddles and repellers on both sides of the originally invariant subspace when there is a symmetry-breaking. As a result, there will be fractal basins both above and below the originally invariant subspace. In higher dimensions, unstable periodic orbits with different unstable dimensions – a type of nonhyperbolicity known as *unstable dimension variability* (see also Sect. 4.4.2), – which are originally all located in the invariant subspace, will be shifted to its neighborhood under a symmetry-breaking perturbation.

For $\varepsilon = 0$, the “roots” of the open set, i.e., the fixed point $(x_p, 0)$ and all its preimages, are located in the invariant subspace $y = 0$ and are dense (see Fig. 5.21a). As we have seen, for $\varepsilon \neq 0$, these “roots” are shifted and are distributed in the two-dimensional phase-space region about $y = 0$, as shown in Fig. 5.21b. Thus, the open set is no longer dense. The set of initial conditions in the unit square $0 \leq (x, y) \leq 1$ that go to the $y = -\infty$ attractor is now open. In fact, it is straightforward to see that the region bounded by the curve $xy < |\varepsilon|/p$ in the unit square maps to $y < 0$ after one iteration. The basin of the $y = -\infty$ attractor in $0 \leq (x, y) \leq 1$ thus consists of this bounded region and all its preimages. The boundaries separating the basins of the $y = \pm\infty$ attractors are fractal. We remark, however, that in this case, the basin in $y > 0$ of the $y = -\infty$ attractor may appear indistinguishable from that of a riddled basin because unstable periodic orbits in the originally invariant subspace are perturbed only slightly.

We thus see that for $p < p_c^0$ and $\varepsilon \neq 0$, persistent chaos in the invariant subspace, together with its riddled basin for $\varepsilon = 0$, is replaced by a chaotic transient and fractal basins of the attractors at infinities, respectively.

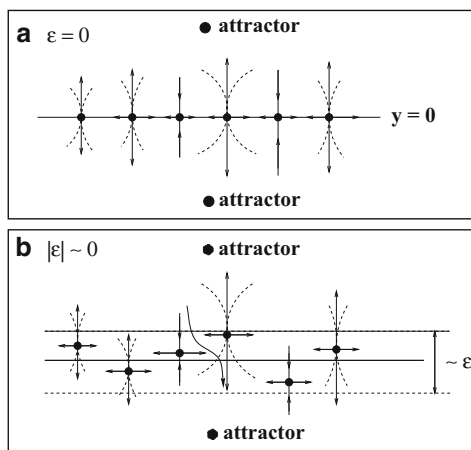


Fig. 5.21 Schematic illustrations of the dynamics of unstable periodic orbits: (a) for $\varepsilon = 0$, $y = 0$ is invariant and the roots of the tongues are dense in $y = 0$, creating a riddled basin; (b) for $\varepsilon \neq 0$, $y = 0$ is no longer invariant, the locations of the periodic orbits are shifted about $y = 0$, and the roots of the tongues are no longer dense, leading to fractal basins [438] (Copyright 1999, the American Physical Society)

5.8.2 Critical Behavior and Scaling Laws

We have seen that the presence of a small amount of symmetry-breaking causes a spread of unstable periodic orbits in a neighborhood of size about ε in the vicinity of the originally invariant subspace. The dynamics outside the neighborhood can be approximately described by that of a random process. To see this, we rewrite (for $y_n > 0$) the y -equation in (5.30), as follows:

$$-\ln y_{n+1} = -\ln y_n - \ln(px_n + \varepsilon/y_n).$$

Letting $Y_n \equiv -\ln y_n$, we obtain

$$Y_{n+1} = Y_n + v_n, \quad (5.32)$$

where $v_n = -\ln(px_n + \varepsilon/y_n)$ is a random variable because x_n comes from a chaotic process. For $\varepsilon \sim 0$, v_n is approximately independent of y_n most of the time (except when y_n gets close to the original invariant subspace). Equation (5.32) thus describes a random walk. If the average drift $v \equiv \langle Y_{n+1} - Y_n \rangle = \langle v_n \rangle$ is small, the random-walk model can be solved using the diffusion approximation, from which various scaling relations can be derived. Specifically, since v is small, the evolution of the probability as a function of discrete time n can be approximated as an evolution in continuous time t . Let $P(Y, t)dY$ be the probability of finding the walker in the interval $[Y, Y + dY]$ at time t . Then $P(Y, t)$ obeys the following diffusion equation [237]:

$$\frac{\partial P}{\partial t} + v \frac{\partial P}{\partial Y} = Q \frac{\partial^2 P}{\partial Y^2}, \quad (5.33)$$

where Q is the diffusion coefficient, defined as

$$2nQ = \langle (Y_n - nv)^2 \rangle. \quad (5.34)$$

Adopting the above diffusive picture, we see that v and Q are the two key parameters that determine the dynamics. In fact, the average drift $-v$ and Q are analogous respectively to the transverse Lyapunov exponent λ_T (which can be defined only when $\varepsilon = 0$) and the diffusion coefficient Q characterizing the degree of the fluctuations of the finite-time transverse Lyapunov exponent, used in Sect. 5.7.3. In the simple model (5.30), $v < 0$ for $p > p_c^0$ and $v > 0$ for $p < p_c^0$. Thus, we have

$$v \sim (p_c^0 - p). \quad (5.35)$$

When there is a symmetry-breaking so that the notions of invariant subspace and transverse Lyapunov exponent no longer hold, we can still use v and Q to characterize the dynamics in the vicinity of the original invariant subspace. In particular, regarding the ε -neighborhood of the original invariant subspace as a *pseudoinvariant manifold* under a symmetry-breaking, the stability of this manifold can be quantified by v and Q . Defining the *pseudotransverse Lyapunov exponent*

$$\Lambda_T \equiv -v, \quad (5.36)$$

we see that if $\Lambda_T > 0$ ($v < 0$), the pseudoinvariant manifold is transversely unstable because a trajectory leaves the pseudoinvariant manifold exponentially rapidly. If, however, $\Lambda_T < 0$ ($v > 0$), a trajectory can spend a long time near the pseudoinvariant manifold, although the trajectory will eventually leave it. In this sense, the manifold is *quasistable* with respect to transverse perturbations. Introducing the pseudotransverse Lyapunov exponent, with the parameter Q characterizing its finite-time fluctuations, thus enables us to quantify the dynamical property of the pseudoinvariant manifold [441].

A detailed discussion about the validity of the diffusion approximation near the transition point to a chaotic attractor with a riddled basin, at which the average drift (or the transverse Lyapunov exponent) is nearly zero, can be found in [565, 567]. Here, because of the symmetry-breaking, the range for the validity of the diffusion approximation is limited. In particular, we note that a trajectory cannot enter the ε -neighborhood of the original invariant subspace $y = 0$. However, for $|y| > |\varepsilon|$, the trajectory experiences both repulsion from and attraction toward the ε -neighborhood of $y = 0$ due to the existence of periodic orbits with different unstable dimensions, namely, repellers and saddles. If $v \approx 0$, the amount of repulsion is approximately equal to that of attraction, and hence we expect the diffusion picture to be valid for $|\varepsilon| < |y| < 1$. This corresponds to the range $Y \in (0, \bar{\varepsilon})$, where $\bar{\varepsilon} = -\ln|\varepsilon| \gg 1$. For clarity of the presentation, we consider the case $\varepsilon < 0$, so that the symmetry-breaking-induced basin of the $y = -\infty$ attractor lies in $y > 0$.

We fix a line segment $0 \leq x \leq 1$ at $y = y_0$, $0 < y_0 \ll 1$, and uniformly choose a large number of initial conditions from it, which leads to the following initial condition for the diffusion equation (5.33):

$$P(Y, 0) = \delta(Y - Y_0), \quad (5.37)$$

where $Y_0 = -\ln y_0$. Since a trajectory reaching $y = 1$ quickly goes to the $y = +\infty$ attractor, we have the following absorbing boundary condition at $Y = -\ln 1 = 0$:

$$P(0, t) = 0. \quad (5.38)$$

Roughly, a trajectory entering the $|\varepsilon|$ -neighborhood of $y = 0$ is lost to the basin of the $-\infty$ attractor. A realistic picture is that the Y -location of the absorbing boundary depends on x . For instance, from the model (5.30), we see that a trajectory goes to the $y = -\infty$ attractor whenever $px_n y_n < |\varepsilon|$. Insofar as x_n is not too small, this happens when $y_n < |\varepsilon|/px_n \sim |\varepsilon|$. Thus, as a crude approximation, we impose another absorbing boundary at $\bar{\varepsilon}$:

$$P(\bar{\varepsilon}, t) = 0. \quad (5.39)$$

Let $F(|\varepsilon|, y_0)$ be the fraction of initial conditions from the line segment at y_0 that go to the $y = -\infty$ attractor A_- . As $|\varepsilon|$ is increased, we expect $F(|\varepsilon|, y_0)$ to increase. For small $|\varepsilon|$, the diffusion equation (5.33) together with the initial and the boundary conditions (5.37)–(5.39) can be solved to yield the following scaling law [441]:

$$F(|\varepsilon|, y_0) = \frac{y_0^{v/Q} - 1}{|\varepsilon|^{v/Q} - 1}. \quad (5.40)$$

If $v > 0$, we have $|\varepsilon|^{v/Q} - 1 \approx -1$ for $|\varepsilon| \ll 1$ and hence $F \approx 1 - y_0^{v/Q} = \text{constant}$, a behavior drastically different from that of the symmetric case (5.27) and (5.28). For $v < 0$, $|\varepsilon|^{v/Q} - 1 \approx |\varepsilon|^{v/Q}$, and hence for any fixed y_0 , we have

$$F(|\varepsilon|, y_0) \sim |\varepsilon|^{-v/Q} = |\varepsilon|^{|v|/Q} \quad \text{for } v < 0. \quad (5.41)$$

We see that in the parameter regime where $v \approx 0$, the fraction remains roughly constant, regardless of the amount of symmetry-breaking. This also implies the catastrophic nature of the symmetry-breaking: riddling is destroyed and a fractal basin component is immediately induced as the system deviates from the symmetric one, no matter how small the deviation is.

Consider a trajectory originated from the symmetry-breaking-induced fractal basin of the $y = -\infty$ attractor in $y > 0$. After it falls into the negative vicinity of $y = 0$, it typically experiences a chaotic transient. In particular, if $v < 0$ ($\Lambda_T > 0$), the transient time is short. If, however, $v > 0$ ($\Lambda_T < 0$), the time can be extraordinarily long [441].

To assess the dimensionality of the boundary between the basin of the $y = +\infty$ attractor and the symmetry-breaking-induced basin, we fix a line segment at $y = y_0$,

where $|\varepsilon| \ll y_0 < 1$, and examine the set of intersecting points with it of the basin boundary. Let d_0 be the box-counting dimension of this set. We expect $0 < d_0 \leq 1$ and the dimension of the boundary to be $D_{b0} = 1 + d_0$ in the two-dimensional phase space. For a riddled basin, D_{b0} is the phase-space dimension. Here, despite the presence of a small amount of symmetry-breaking, D_{b0} is still close to 2. *Thus, in a practical sense, the symmetry-breaking-induced fractal basin resembles a riddled one.*⁴

It can be shown, utilizing the solution to the diffusion equation (5.33) [441, 565, 567], that the uncertainty exponent is independent of the symmetry-breaking parameter ε and is given by

$$\alpha = \frac{v^2}{4Q\lambda_1}, \quad (5.42)$$

where λ_1 is the Lyapunov exponent on the original attractor \mathcal{A} in the invariant subspace. Thus, in the regime where $v \approx 0$ (but $v \neq 0$), so that the diffusion approximation is valid, we expect $\alpha \approx 0$ and hence $d_0 \approx 1$, leading to

$$D_{b0} = 2 - \frac{v^2}{4Q\lambda_1}.$$

A fractal basin boundary with dimension close to that of the phase space (or a near-zero uncertainty exponent) means that the uncertainty probability remains approximately constant, regardless of how accurately we can specify the initial condition. Thus, realistically, it is impossible to predict, from a given initial condition, the asymptotic attractor. This fundamental obstacle to prediction is common for riddled basins and persists even when the riddled basin is replaced by a fractal one due to symmetry-breaking.

⁴ Since very close to a boundary arises the chaotic saddles's stable manifold is nearly space-filling, the set of initial conditions leading to long transients also exhibits riddled-like behavior [834]